1. 急性白血病

間 野 博 行

急性白血病の治療戦略は，アントラサイクリン＋シトシンアラビノシドを中心とする化学療法と骨髄移植療法とを2本柱としたプロトコールで組み立てられてきた．しかし近年，白血病の病態解明と臨床データが蓄積されるに従い，各患者個人に最適化された治療スケジュールの構築が求められている．急性白血病はきわめて多様な病因・臨床像からなるいわば症候群のようなものであるため，白血病患者への治療法の最適化のためには，白血病の成因・予後因子に応じた形での新たな患者層別化が必要であろう．そのよい例としてt(15;17) を有する急性前骨髄球性白血病（APL）があげられる．この染色体転座の結果，レチノイン酸受容体（RAR α）とPMLとの融合蛋白質が産生されるが，本分子を標的としたall-trans retinoic acidはAPLの寛解導入に著効するのである．

これまで急性白血病の分類には，主に白血病細胞の形態学を基盤としたFrench–American–Britishグループ（FAB）分類[1] が利用されてきたが，近年の遺伝子解析の知見を取り入れたWorld Health Organization（WHO）分類が1999年に提唱された[2]．しかしながら，これらの分類法は各患者の予後予測にはいまだ不充分であり，たとえばDNAマイクロアレイによる網羅的発現解析データを取り入れる工夫などが試みられている．

まの ひろゆき／自治医科大学ゲノム機能研究部教授

急性骨髄性白血病（AML）

旧来のFAB分類では，APLに相当するM3サブタイプが予後良好なこと，また未分化なタイプのM0および赤白血病M6，巨核芽球性白血病M7が予後不良なことが知られていた．しかしながら，症例数の多いM1やM4サブタイプの患者予後は均一ではなく，新たな層別化のマーカーが待たれていた．その後，AMLにおいてしばしば観察される染色体転座の原因遺伝子が同定され，これら染色体異常と各患者予後との詳細な解析がなされるに至った．

現段階では，これらの知見を取り入れた核型による患者層別化がシンプルでかつAMLの予後予測に最も有効なものといえる．Medical Research Council（MRC）による1,600例に及ぶAML患者の核型解析の結果，表1に示される患者層別化が

表1 核型に基づくAMLサブグループの層別化

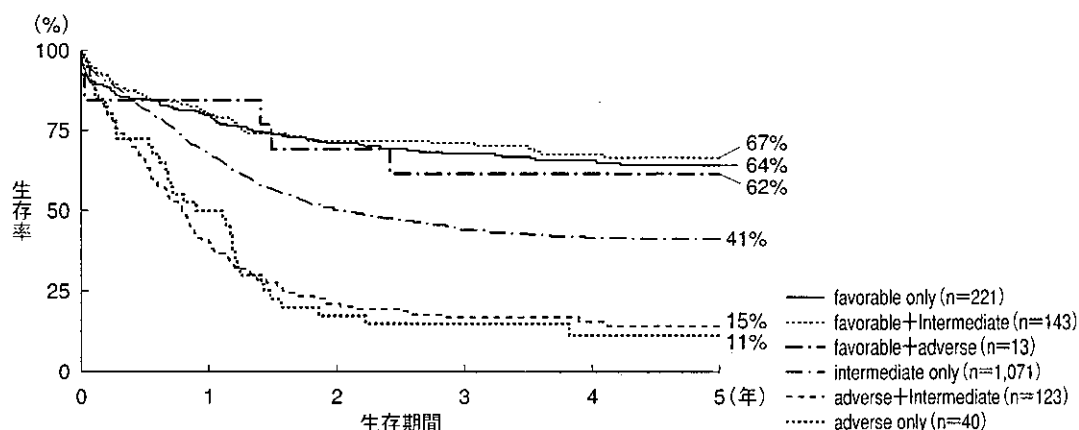| グループ	核 型
favorable	t(8;21) t(15;17) inv(16)
intermediate	all others
adverse	−5/del(5q) −7 abnormal 3q complex

図1 核型による患者生命予後（文献3より改変）
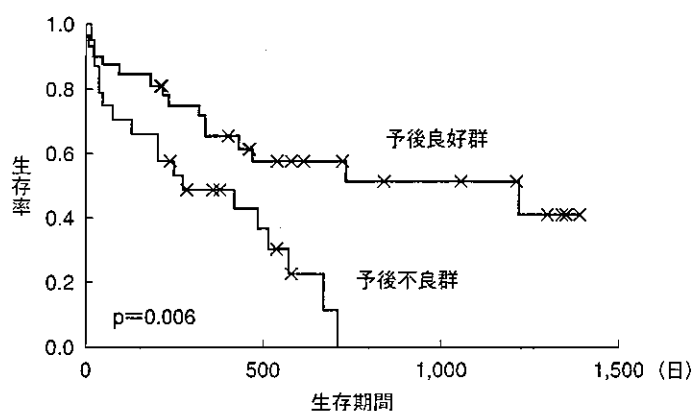表1に示されるfavorable，intermediate，adoverse各患者グループの生存曲腺をKaplan-Meier解析で示す．3群の長期生存率が大きく異なることがわかる．

図2 DNAマイクロアレイによる層別化（文献5より改変）
DNAマイクロアレイ解析の結果同定された「予後にリンクする遺伝子セット」の発現量を用いて，患者を2群に分類した．両群間の生存曲腺が大きく異なることをKaplan-Meier解析で示す．

提案された[3]．予後良好なfavorable groupに属するt(15;17)，t(8;21) およびinv(16) は，それぞれFAB分類におけるM3，M2およびM4 Eoに相当する．また，intermediate groupに属する11q23転座はMLL遺伝子の変化を含むことが多い．一方，monosomy 7および5q−は重要な予後不良因子であるが，本核型異常において具体的に

どの遺伝子の量的変化が重要なのかは全く不明なままである．これら核型による予後予測はきわめて強力であり，たとえば表1の各グループの長期生命予後を比較すると図1の生存曲線に示されるとおり，3群は大きく異なる予後を有することが明らかである．なお，「正常核型」が予後良好群ではなくintermediate groupに属することは注意すべきであろう．

核型による分類だけでは，AML患者の約半数を占める正常核型を有する患者の層別化が困難である．そこで核型以外のさまざまなパラメータも単変量あるいは多変量解析によって検討されてきた．たとえばJapan Adult Leukemia Study Group (JALSG) の解析では，年齢，芽球のmyeloperoxidase陽性率，performance status，末梢血白血球数，血球の異形成の有無などが生存に有意にリンクすることが報告されている[4]．

近年では，DNAマイクロアレイを用いた網羅

的遺伝子発現データによってAML芽球の遺伝子発現プロファイルをとらえ，そのパターンから予後を予測する試みもなされている．たとえばBullingerらは，26,260種類の遺伝子が配置されたDNAマイクロアレイを用いて，116例のAML検体（骨髄あるいは末梢血単核球）の遺伝子発現データを得た[5]．これらの遺伝子中，患者予後にリンクするもの133種類を抽出し，その発現プロファイルから患者を大きく2群に分けている．その結果図2に示されるように，両患者グループの長期予後は有意に異なることが明らかになった．しかもこれら遺伝子データによる分類は，正常核型の患者内でも予後が異なる2群が存在することを示しており，発現プロファイルによる分類が旧来の核型分類とは異なる情報を与えるといえる．

急性リンパ性白血病（ALL）

小児のALLがきわめて予後良好な白血病であるのに比し，成人のALLは一般に予後不良である．ALLはFAB分類によりL1，L2，L3の3種類に分類されてきた．L3は本邦ではまれなBurkittリンパ腫型であり，実際はL1とL2が大部分を占める．今日の治療において患者の生命予後にL1とL2の区別はリンクしておらず，新しいWHO分類でもL1，L2，L3のサブタイプは却下された．

成人ALLの予後予測因子を解析した報告は多くないが，AMLの場合と同様に核型が重要な指標となる．Cancer and Leukemia Group B（CALGB）による256例の解析では，t(9;22)，t(4;11)，monosomy 7，trisomy 8の存在が長期生存に対する予後不良因子であることが示された[6]．さらに高齢，初診時の白血球数高値，B細胞系芽球なども同様な予後不良因子であるとされている．また，JALSGによる本邦ALL症例の解析でも，t(9;22)の存在と高齢（30歳以上），白血球数高値（3万/mm^3以上）が予後不良因子であると報告された[7]．

●おわりに

核型による層別化がきわめて有効なのは，急性白血病が多様な症候群であり，その病因単位に治療法を最適化するべきであることを示唆しているといえよう．白血病の成因が漸次明らかになるに伴い，層別化がさらに細分化されるとともに，各病因に対応した分子標的療法が開発されると期待される．一方，病因の多くが不明な今日においては，それを間接的に評価可能なDNAマイクロアレイ解析が有効なツールとなるのではないだろうか．

文 献

1) Bennett JM, Catovsky D, Daniel MT, et al. Proposed revised criteria for the classification of acute myeloid leukemia. A report of the French-American-British Cooperative Group. Ann Intern Med 1985; 103: 620-5.
2) Jaffe ES, Harris NL, Stein H, et al, editors. Tumours of haematopoietic and lymphoid tissues. Lyon: IARCPress; 2001.
3) Grimwade D, Walker H, Oliver F, et al. The importance of diagnostic cytogenetics on outcome in AML: analysis of 1612 patients entered into the MRC AML10 trial. Blood 1998; 92: 2322-33.
4) 栗山一孝, 吉田真一郎, 今西大介, 他. JALSGにおけるAML化学療法. 臨床血液 1988; 39: 98-102.
5) Bullinger L, Dohner K, Bair E, et al. Use of gene-expression profiling to identify prognostic subclasses in adult acute myeloid leukemia. N Engl J Med 2004; 350: 1605-16.
6) Wetzler M, Dodge RK, Mrozek K, et al. Prospective karyotype analysis in adult acute lymphoblastic leukemia: The Cancer and Leukemia Group B experience. Blood 1999; 93: 3983-93.
7) Takeuchi J, Kyo T, Naito K, et al. Induction therapy by frequent administration of doxorubicin with four other drugs, followed by intensive consolidation and maintenance therapy for adult acute lymphoblastic leukemia: the JALSG-ALL93 study. Leukemia 2002; 16: 1259-66.

Overexpression of A Hybrid Gene Consisting of The Amino-Terminal Fragment of Urokinase and Carboxyl-Terminal Domain of Bikunin Suppresses Invasion and Migration of Human Ovarian Cancer Cells *In Vitro*

Yuji Takei[1,2], Hiroaki Mizukami[2], Yasushi Saga[1], Hiroshi Kobayashi[3], Mika Suzuki[3], Takashi Matsushita[2], Keiya Ozawa[2] and Mitsuaki Suzuki[1]*

[1]*Department of Obstetrics and Gynecology, Jichi Medical School, Tochigi, Japan*
[2]*Division of Genetics Therapeutics, Center for Molecular Medicine, Jichi Medical School, Tochigi, Japan*
[3]*Department of Obstetrics and Gynecology, Hamamatsu University School of Medicine, Shizuoka, Japan*

A Kunitz-type protease inhibitor, bikunin, is known to suppress the invasion and metastasis of cancer cells. HI8, a carboxyl-terminal domain of bikunin, is an active site of this glycoprotein. To increase its affinity for cancer cells, we constructed a chimeric gene, *ATF-HI8*, and investigated the anti-invasive and anti-migratory activity of *ATF-HI8* on ovarian cancer cells. ATF-HI8-expressing plasmid and ATF-expressing plasmid were introduced into the highly invasive and metastatic ovarian cancer cell line HRA. The properties of the established cell line (HRA/ATF-HI8) were compared to those of the HRA/ATF and the HRA/luciferase (HRA/LUC, control) cell lines in terms of cell proliferation, invasion and migration. As a result, (i) there were no differences in cell proliferation between HRA/ATF-HI8 and HRA/LUC; (ii) the invasion and migration of HRA/ATF-HI8 cells were significantly inhibited compared to those of HRA/LUC cells; (iii) the migration, but not the invasion, of HRA/ATF cells was significantly inhibited compared to that of HRA/LUC. These results indicate that the overexpression of *ATF-HI8* inhibits the invasion and migration of ovarian cancer cells without affecting cell proliferation and suggest that HI8 is involved in the anti-invasive and the anti-migratory activities, and the addition of *ATF* brought about the increase in the anti-migratory activity of HI8. The above findings suggest the applicability of therapeutic strategies targeting the inhibition of peritoneal invasion and dissemination of ovarian cancer by the use of the chimeric gene *ATF-HI8*.
© 2004 Wiley-Liss, Inc.

Bikunin is a physiologically active glycoprotein with a molecular weight of approximately 40 kD occurring in human amniotic fluid and urine and in lower concentrations in blood. It inhibits trypsin, chymotrypsin, plasmin and elastase and is used to treat acute pancreatitis and acute circulatory failure as a drug. HI8, a carboxyl-terminal domain of bikunin, is an active site for this glycoprotein. In addition, bikunin is known to suppress the invasion and metastasis of cancer cells. The mechanism of suppression is thought to involve inhibiting the activity of plasmin on the cancer cell surface and the production of urokinase-type plasminogen activator (uPA), thereby suppressing the destruction of extracellular matrix and the basement membrane of vascular endothelial cells and tumor cells, resulting in the inhibition of cancer cell invasion and metastasis.[1–5] Since high-affinity receptors for bikunin are not found on the surface of cancer cells, enhancement of its affinity for cancer cells is necessary to increase its effectiveness. It is known that the affinity of uPA for uPA receptors (uPAR) is approximately 500 times higher than that of bikunin for bikunin receptors.[6,7] Therefore, we focused our attention on the amino-terminal fragment (ATF) of uPA, the receptor-binding site, under the speculation that linking ATF to HI8 would increase the affinity of HI8 to the cancer cell surface. We have previously purified a chimeric protein consisting of ATF linked to HI8 and confirmed that exogenous ATF-HI8 could inhibit cancer cell invasion and metastasis.[7,8] The plasmid used for purification of ATF-HI8 chimeric protein had no signal sequence. In our study, we added a signal sequence to the plasmid and could cause the human cells to secrete the ATF-HI8 chimeric protein. The purpose of our study

was to construct the chimeric gene *ATF-HI8* and to investigate whether it inhibits ovarian cancer cell invasion and migration.

Material and methods

Plasmid construction

Total RNA was extracted from human placental tissue, and a human placenta cDNA library was constructed by RT-PCR. The *ATF* cDNA was cloned by PCR using the human placenta cDNA library. The *HI8* cDNA was cloned by PCR using the bikunin cDNA,[9] which was cloned from human liver cDNA and kindly provided by Dr. Hiroshi Itoh at Miyazaki Medical College. The following primers containing relevant restriction sites were used to amplify the cDNA for *ATF* and *HI8*. Primer 1 (5'-CGCGGATC-CACCTCGCCACCATGAGAGCCCTGCTG-3') and primer 2 (5'-GGGGTACCATCTGCGCAGTCATGCACCATGCA-3') are primers for *ATF* cDNA. Primer 3 (5'-GGGGTACCGTGGCGG-CCTGCAATCTCCCCATAGTCCG-3') and primer 4 (5'-GCT-CTAGATCAGTTGGAGAAGCGCAGCAGCTCCTCAT-3') are primers for *HI8* cDNA. After several intermediate steps, a BamHI-*ATF*-KpnI-*HI8*-XbaI fragment was subcloned into pCMV-IRES-bsr.[10] Similarly, BamHI-*ATF*-KpnI fragment was subcloned into pCMV-IRES-bsr.

Transfection into HRA cell line

The human ovarian serous carcinoma cell line HRA was provided by Prof. Y. Kikuchi and was cultured as described previously.[11]

pCMV-ATF-HI8-IRES-bsr, pCMV-ATF-IRES-bsr and the control plasmid pCMV-luciferase (LUC)-IRES-bsr[10] encoding *LUC* were transfected into HRA cells by the standard calcium phosphate precipitation method.[12] The cells were selected in the presence of 10 μg/ml of blasticidin S hydrochloride(Funakoshi, Tokyo, Japan). Resistant cells were obtained after 4 weeks. HRA/ATF-HI8, HRA/ATF and HRA/LUC were subsequently maintained in the presence of 10 μg/ml of blasticidin S hydrochloride.

Western blotting

HRA/ATF-HI8 and HRA/LUC were plated in 10 cm plastic dishes and cultured in serum-free DMEM/F-12 medium. The supernatant was collected 24 hr later and subjected to electrophoresis. Western blotting was performed by standard procedures[13] with either anti-uPA-A chain antibody to detect the ATF portion of the

chimeric protein or anti-inter-alpha-trypsin inhibitor antibody (Da-koCytomation A/S, Copenhagen, Denmark) to detect the HI8 portion. Anti-mouse antibody and anti-rabbit antibody were used as the second antibodies, respectively. The reactions were visualized using an ECL Detection System (Amersham Biosciences, Piscataway, NJ).

In vitro *cell growth kinetics*

HRA/ATF-HI8 and HRA/LUC were plated in 6-well plates at 5 × 10⁴ cells/well and cultured in 10% serum-supplemented DMEM/F-12 medium. For each group, the cells in 1 well were dislodged with 0.05% trypsin-EDTA every 24 hr and were counted using a hemocytometer. This experiment was performed in triplicate.

In vitro *invasion assay*

The methods for testing tumor cell invasion were essentially the same as previously described.[1-3,5,14,15]. In our study, a BD BioCoat Matrigel Invasion Chamber (Becton Dickinson, Franklin Lakes, NJ) was used to measure cell invasion. Medium containing 5 μg/750 μl of fibronectin was added to each well. Cells (2 × 10⁵) were resuspended in 2% serum-supplemented DMEM/F-12 (500 μl) and seeded into the upper chamber. After incubation for 20 hr at 37°C, the chamber was stained and the number of cells invaded into the Matrigel-coated membranes was counted. We counted the cells in 5 high-power fields.

In vitro *scratch wound healing assay*

Cell migration was measured by the *in vitro* scratch wound healing assay.[16] Monolayer cells were scratched with a sterile pipette tip in 10 cm plastic dishes, and after 8 hr of culture in 2% serum-supplemented DMEM/F-12, the cell migration was evaluated by counting cells that migrated from the wound edge.

Statistical analysis

All experiments were independently repeated twice or more. The significance of differences was analyzed by unpaired Student's t-test. The ANOVA and the post-hoc tests were used for comparison among the 3 groups. A value of $p < 0.05$ was regarded as significant.

Results

Construction of the chimeric gene ATF-HI8 and its expression in HRA cells

We constructed the chimeric gene *ATF-HI8*, which was 675 bp long, containing a signal sequence to be a secretable protein.

The ATF-HI8 expression plasmid pCMV-ATF-HI8-IRES-bsr, the ATF expression plasmid pCMV-ATF-IRES-bsr and the control plasmid pCMV-LUC-IRES-bsr (Fig. 1) were each transfected into HRA cells. As shown in Figure 2, ATF-HI8 expression was detected by Western blotting at the position corresponding to a molecular weight of 22 kD in the culture supernatant of HRA/ATF-HI8, while no ATF-HI8 expression was detected in the culture supernatant of HRA/LUC.

In vitro *cell growth kinetics*

The growth curves of HRA/ATF-HI8 and HRA/LUC are shown in Figure 3. There were no significant differences in growth between the 2 cell lines. Therefore, expression of the *ATF-HI8* gene did not affect the cell growth *in vitro*.

In vitro *invasion assay*

The effects of *ATF-HI8* expression on cell invasion *in vitro* are shown in Figure 4. ATF-HI8-expressing cells exhibited decreased invasion. The number of HRA/ATF-HI8 cells that invaded through the filter was 77 ± 24/HPF, which was significantly lower than that of HRA/LUC (202 ± 52/HPF, $p < 0.02$). No significant difference was noted between the numbers of HRA/ATF (119 ± 7/HPF) and HRA/LUC.

In vitro *scratch wound healing assay*

The effects of *ATF-HI8* expression on cell migration *in vitro* are shown in Figure 5. ATF-HI8-expressing cells exhibited decreased migration. The number of HRA/ATF-HI8 cells migrating to the scratched area was 198 ± 33/scratched area, which was significantly lower than those of HRA/ATF (381 ± 72/scratched area,

pCMV-ATF-HI8-IRES-bsr

BamHI   KpnI   XbaI

| CMV | — | ATF | HI8 | — | IRES | — | bsr |

pCMV-ATF-IRES-bsr

BamHI   KpnI
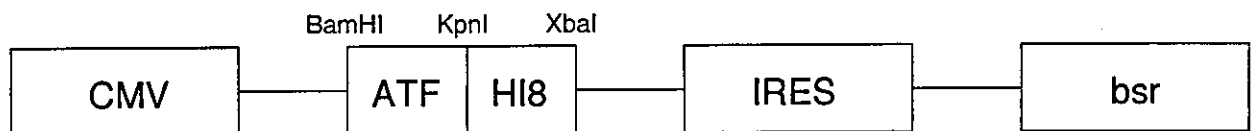
| CMV | — | ATF | — | IRES | — | bsr |
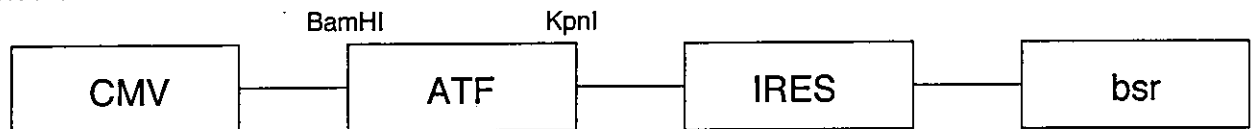
pCMV-LUC-IRES-bsr
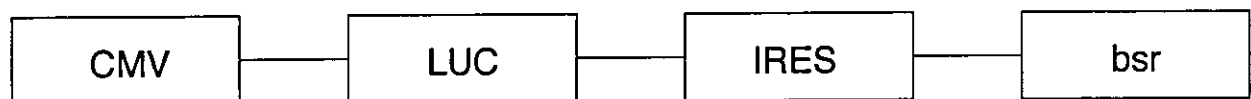
| CMV | — | LUC | — | IRES | — | bsr |

FIGURE 1 – Schematic representation of the construction of the ATF-HI8 expression plasmid vector (pCMV-ATF-HI8-IRES-bsr), ATF expression plasmid vector (pCMV-ATF-IRES-bsr) and control plasmid vector (pCMV-LUC-IRES-bsr) in a simple style. CMV, cytomegalovirus promotor; IRES, internal ribosome entry site; bsr, blasticidin S-resistant gene; LUC, luciferase.
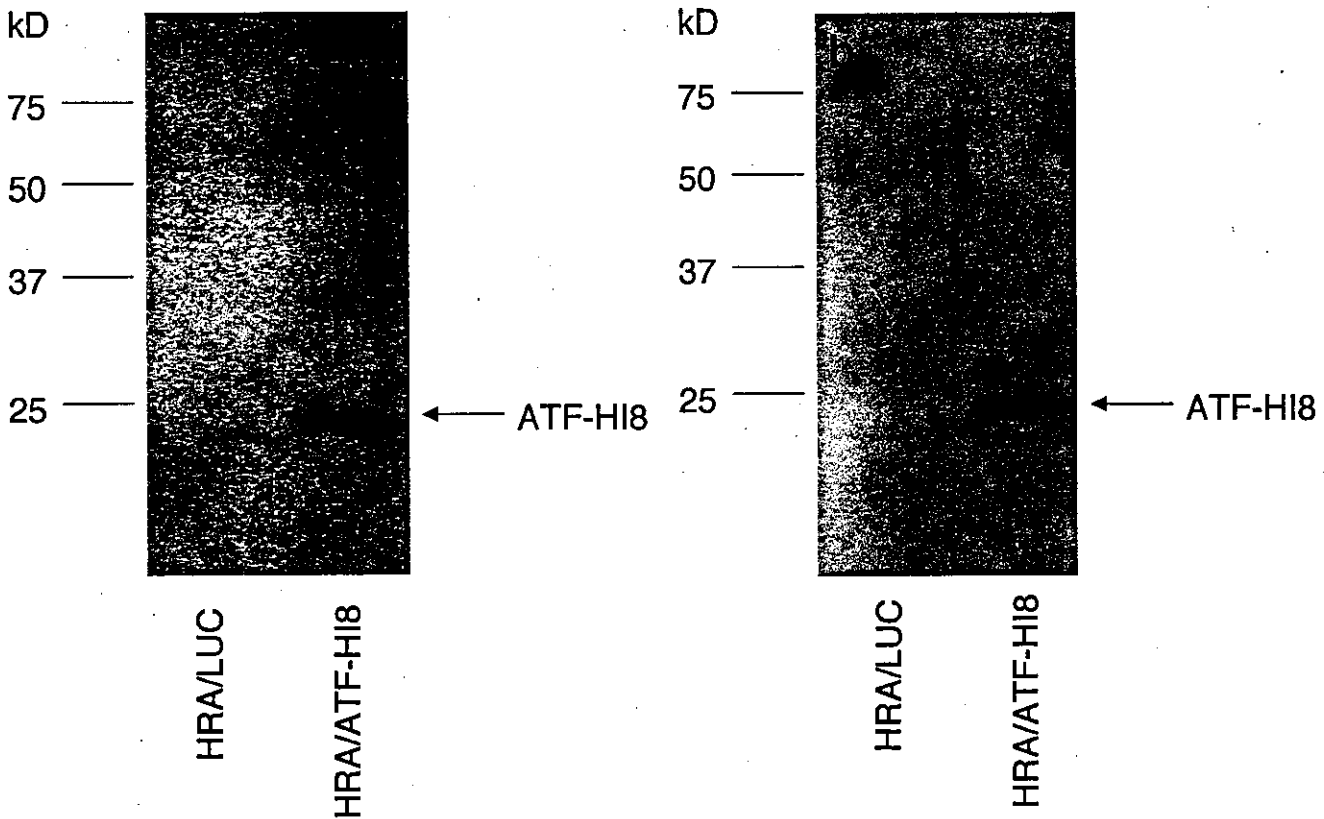
FIGURE 2 – Detection of ATF-HI8 in culture supernatant by Western blotting using anti-uPA-A chain antibody *(a)* and anti-inter-alpha-trypsin inhibitor antibody *(b)*. ATF-HI8 expression was detected at a position corresponding to 22 kD. Molecular weight standards are indicated on the left of each figure.
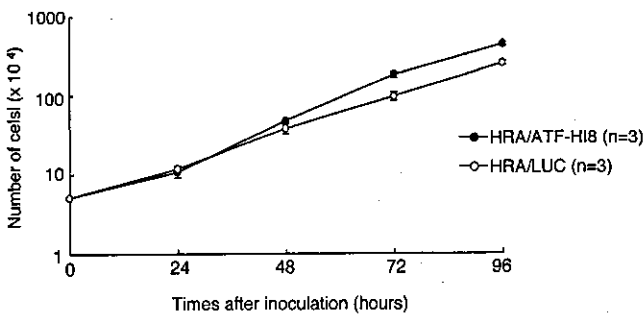

Times after inoculation (hours)

FIGURE 3 – The growth curves of HRA/ATF-HI8 and HRA/LUC. This experiment was independently repeated twice.

$p < 0.05$) and HRA/LUC cells (632 ± 78/scratched area, $p < 0.001$). The migration of HRA/ATF cells was significantly inhibited compared to that of HRA/LUC cells ($p < 0.01$).

Discussion

In our study, we constructed the chimeric gene *ATF-HI8*, introduced it into the ovarian cancer cell line HRA and examined the influence of *ATF-HI8* expression on the cellular proliferation, invasion and migration properties.

The results showed that the overexpression of *ATF-HI8* inhibited the invasion and migration of ovarian cancer cells and that the expression of *ATF* alone inhibited the migration but not the invasion. Therefore, we speculate that *HI8* is involved in the anti-invasive and the anti-migratory activities, and the addition of *ATF*

brought about the increase in the anti-migratory activity of *HI8*. ATF prevents uPA from binding to the uPAR. uPA is known to be localized on the leading edge of migrating cells and to facilitate the dissolution of extracellular matrix by activating plasmin to allow cell migration. It has been reported that ATF competitively blocks the binding of uPA to uPAR, resulting in inhibition of the dissolution of extracellular matrix, leading to suppression of cell migration.[17–20] To extend this approach, attempts to construct chimeric genes such as *TIMP-1.ATF* have been made in the cardiovascular field, mainly to prevent the restenosis of the vessel lumen.[21–23]

What is the clinical relevance of the anti-migratory activity, one of the two activities of the chimeric gene *ATF-HI8*? Recently, we introduced *HGF/NK4*, a hepatocyte growth factor *(HGF)* antagonist, into an ovarian cancer cell line and showed that *HGF/NK4* overexpression inhibits ovarian cancer cell migration *in vitro* and peritoneal dissemination *in vivo*.[24] Thus, it is considered that cell migration is one of the critical factors that directs peritoneal dissemination and that the inhibition of cell migration could control peritoneal dissemination. Therefore, the present observation also suggests that *ATF-HI8* overexpression exerts an inhibitory effect not only on invasion but also on peritoneal disseminated metastasis of ovarian cancer.

As the body of work reflects the potential utility of *ATF-HI8* in ovarian cancer therapy, a more practical experiment should be designed to prove the clinical relevancy. For this purpose, long-term expression of *ATF-HI8* is essential, and adeno-associated virus (AAV)-mediated gene transfer into normal tissue would be a reasonable choice. Since AAV vector can transduce normal tissues such as muscle and liver,[25–28] the AAV vector-mediated administration of *ATF-HI8* may lead to a clinical benefit.
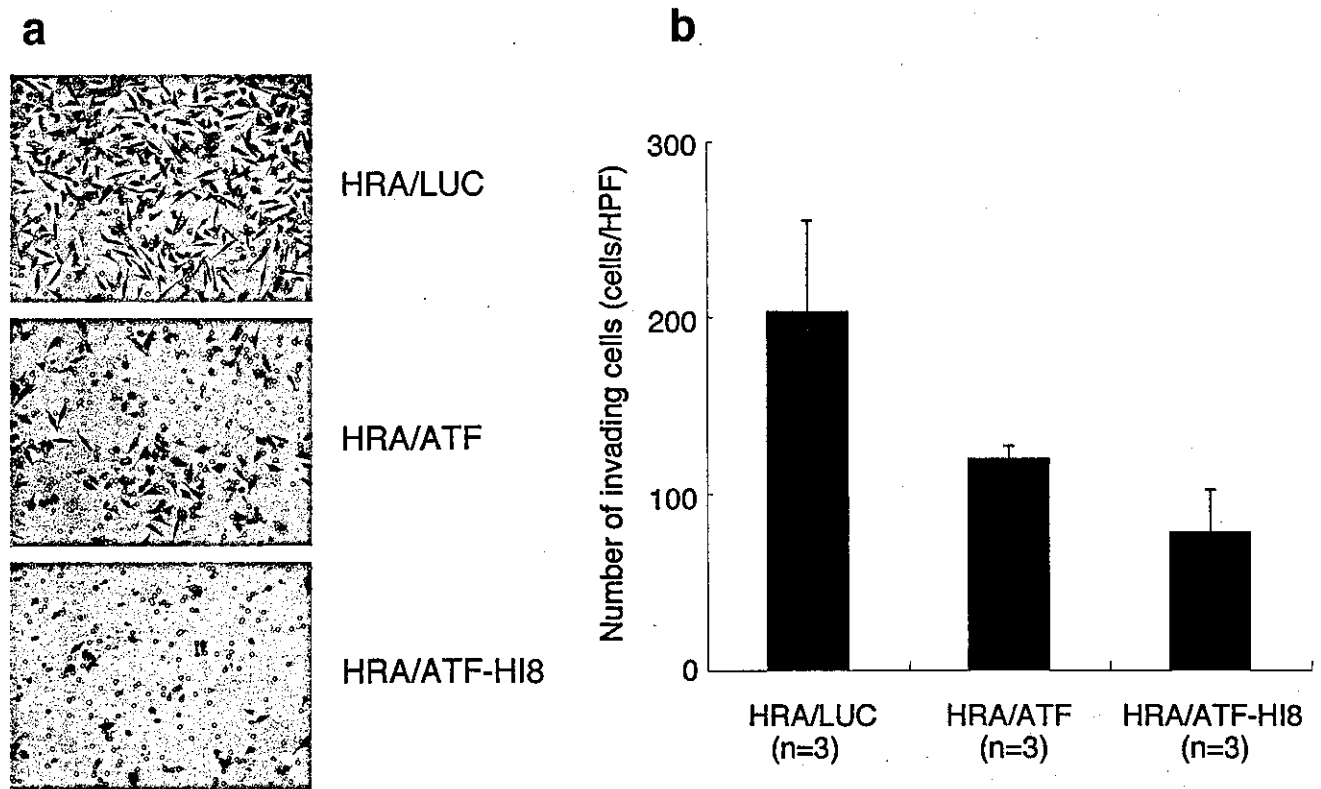
a

b

FIGURE 4 – Cell invasion of HRA/ATF-HI8, HRA/ATF and HRA/LUC in the *in vitro* invasion assay. *(a)* Light micrograph of cells invading through the filter onto its undersurface. *(b)* The number of HRA/ATF-HI8 cells invading was 77 ± 24/HPF, which was significantly lower than that of HRA/LUC cells (202 ± 52/HPF, $p < 0.02$). There was no significant difference between HRA/ATF (119 ± 7/HPF) and HRA/LUC.

a

b

X 40   X 100
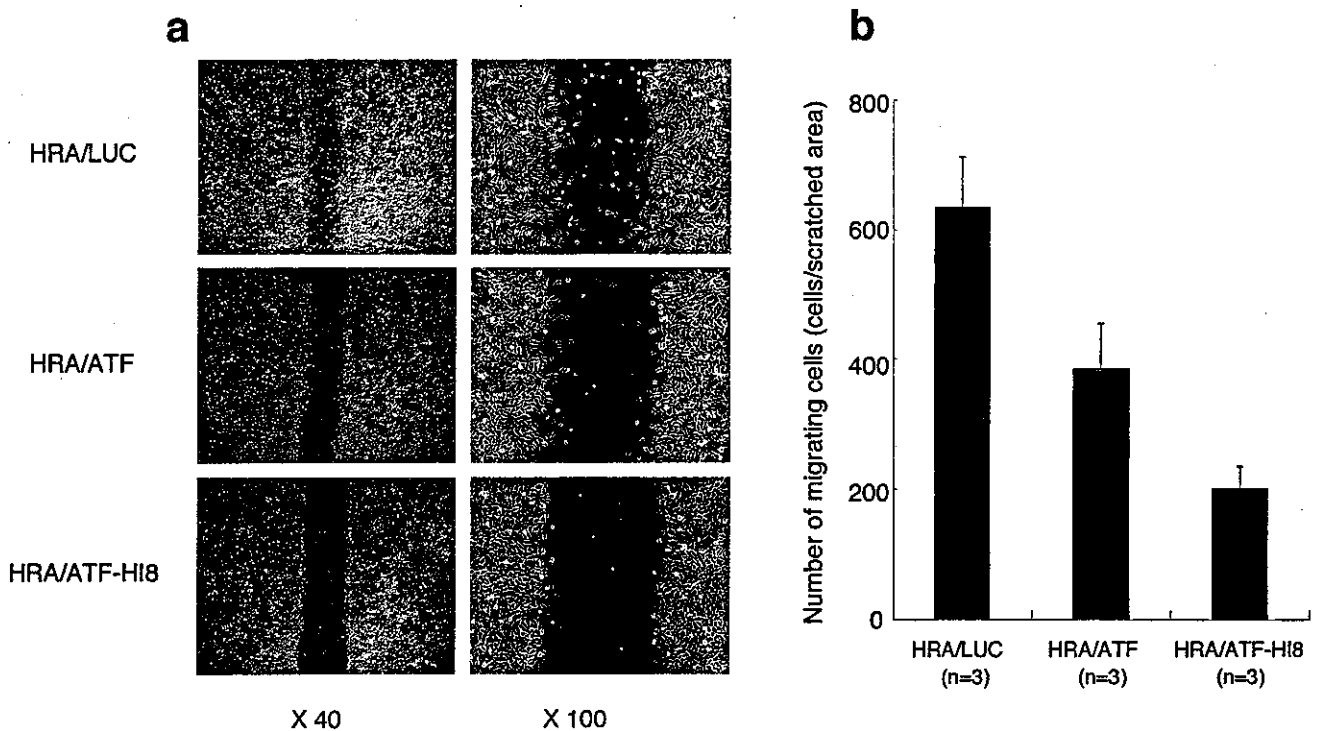
FIGURE 5 – Cell migration of HRA/ATF-HI8, HRA/ATF and HRA/LUC in the *in vitro* scratch wound healing assay. *(a)* Light micrograph of migrating cells. *(b)* The number of HRA/ATF-HI8 cells migrating 8 hr after scratching was 198 ± 33/scratched area, which was significantly lower than those of HRA/ATF (381 ± 72/scratched area, $p < 0.05$) and HRA/LUC cells (632 ± 78/scratched area, $p < 0.001$). The cell number of HRA/ATF was significantly lower than that of HRA/LUC ($p < 0.01$).

In conclusion, we constructed a chimeric gene that expresses and secretes ATF-HI8 and showed that *ATF-HI8* overexpression inhibited the invasion and migration of ovarian cancer cells. These findings may lead to the development of gene therapy with the *ATF-HI8* gene targeting peritoneal invasion and disseminated metastasis of ovarian cancer.

References

1. Kobayashi H, Fujie M, Shinohara H, Ohi H, Sugimura M, Terao T. Effect of urinary trypsin inhibitor on the invasion of reconstituted basement membranes by ovarian cancer cells. Int J Cancer 1994;57: 378–84.
2. Kobayashi H, Shinohara H, Takeuchi K, Itoh M, Fujie M, Saitoh M, Terao T. Inhibition of the soluble and the tumor cell receptor-bound plasmin by urinary trypsin inhibitor and subsequent effects on tumor cell invasion and metastasis. Cancer Res 1994;54:844–9.
3. Kobayashi H, Shinohara H, Ohi H, Sugimura M, Terao T, Fujie M. Urinary trypsin inhibitor (UTI) and fragments derived from UTI by limited proteolysis efficiently inhibit tumor cell invasion. Clin Exp Metastasis 1994;12:117–28.
4. Kobayashi H, Gotoh J, Fujie M, Terao T. Characterization of the cellular binding site for the urinary trypsin inhibitor. J Biol Chem 1994;269:20642–7.
5. Kobayashi H, Gotoh J, Kanayama N, Hirashima Y, Terao T, Sugino D. Inhibition of tumor cell invasion through matrigel by a peptide derived from the domain II region in urinary trypsin inhibitor. Cancer Res 1995;55:1847–52.
6. Kobayashi H, Gotoh J, Hirashima Y, Fujie M, Sugino D, Terao T. Inhibitory effect of a conjugate between human urokinase and urinary trypsin inhibitor on tumor cell invasion in vitro. J Biol Chem 1995; 270:8361–6.
7. Kobayashi H, Sugino D, She MY, Ohi H, Hirashima Y, Shinohara H, Fujie M, Shibata K, Terao T. A bifunctional hybrid molecule of the amino-terminal fragment of urokinase and domain II of bikunin efficiently inhibits tumor cell invasion and metastasis. Eur J Biochem 1998;253:817–26.
8. Sugino D, Okushima M, Kobayashi H, Terao T. Production of a hybrid protein consisting of the N-terminal fragment of urokinase and the C-terminal domain of urinary trypsin inhibitor in Escherichia coli. Biotechnol Appl Biochem 1998;27:145–52.
9. Suzuki M, Kobayashi H, Tanaka Y, Hirashima Y, Kanayama N, Takei Y, Saga Y, Suzuki M, Itoh H, Terao T. Suppression of invasion and peritoneal carcinomatosis of ovarian cancer cell line by overexpression of bikunin. Int J Cancer 2003;104:289–302.
10. Urabe M, Hasumi Y, Ogasawara Y, Matsushita T, Kamoshita N, Nomoto A, Colosi P, Kurtzman GJ, Tobita K, Ozawa K. A novel dicistronic AAV vector using a short IRES segment derived from hepatitis C virus genome. Gene 1997;200:157–62.
11. Kikuchi Y, Kizawa I, Oomari K, Miyauchi M, Kita T, Sugita M, Tenjin Y, Kato K. Establishment of a human ovarian cancer cell line capable of forming ascites in nude mice and effects of tranexamic acid on cell proliferation and ascites formation. Cancer Res 1987;47: 592–6.
12. Wigler M, Pellicer A, Silverstein S, Axel R. Biochemical transfer of single-copy eucaryotic genes using total cellular DNA as donor. Cell 1978;14:725–31.
13. Laemmli UK. Cleavage of structural proteins during the assembly of the head of bacteriophage T4. Nature 1970;227:680–5.
14. Kobayashi H, Gotoh J, Fujie M, Shinohara H, Moniwa N, Terao T. Inhibition of metastasis of Lewis lung carcinoma by a synthetic peptide within growth factor-like domain of urokinase in the experimental and spontaneous metastasis model. Int J Cancer 1994;57:727– 33.
15. Kobayashi H, Moniwa N, Sugimura M, Shinohara H, Ohi H, Terao T. Effects of membrane-associated cathepsin B on the activation of receptor-bound prourokinase and subsequent invasion of reconstituted basement membranes. Biochim Biophys Acta 1993;1178:55–62.

16. Tamura M, Gu J, Matsumoto K, Aota S, Parsons R, Yamada KM. Inhibition of cell migration, spreading, and focal adhesions by tumor suppressor PTEN. Science 1998;280:1614–7.
17. Mohanam S, Chandrasekar N, Yanamandra N, Khawar S, Mirza F, Dinh DH, Olivero WC, Rao JS. Modulation of invasive properties of human glioblastoma cells stably expressing amino-terminal fragment of urokinase-type plasminogen activator. Oncogene 2002;21:7824– 30.
18. Dear AE, Medcalf RL. The urokinase-type-plasminogen-activator receptor (CD87) is a pleiotropic molecule. Eur J Biochem 1998;252: 185–93.
19. Li H, Lu H, Griscelli F, Opolon P, Sun LQ, Ragot T, Legrand Y, Belin D, Soria J, Soria C, Perricaudet M, Yeh P. Adenovirus-mediated delivery of a uPA/uPAR antagonist suppresses angiogenesis-dependent tumor growth and dissemination in mice. Gene Ther 1998;5: 1105–13.
20. Li H, Griscelli F, Lindenmeyer F, Opolon P, Sun LQ, Connault E, Soria J, Soria C, Perricaudet M, Yeh P, Lu H. Systemic delivery of antiangiogenic adenovirus AdmATF induces liver resistance to metastasis and prolongs survival of mice. Hum Gene Ther 1999;10: 3045–53.
21. Lamfers ML, Grimbergen JM, Aalders MC, Havenga MJ, de Vries MR, Huisman LG, van Hinsbergh VW, QuaxPH. Gene transfer of urokinase-type plasminogen activator receptor-targeted matrix metalloproteinase inhibitor TIMP-1.ATF suppresses neointima formation more efficiently than tissue inhibitor of metalloproteinase-1. Circ Res 2002;91:945–52.
22. QuaxPH, Lamfers ML, Lardenoye JH, Grimbergen JM, de Vries MR, Slomp J, de Ruiter MC, Kockx MM, Verheijen JH, van Hinsbergh VW. Adenoviral expression of a urokinase receptor-targeted protease inhibitor inhibits neointima formation in murine and human blood vessels. Circulation 2001;103:562–9.
23. Lamfers ML, Wijnberg MJ, Grimbergen JM, Huisman LG, Aalders MC, Cohen FN, Verheijen JH, van Hinsbergh VW, QuaxPH. Adenoviral gene transfer of a u-PA receptor-binding plasmin inhibitor and green fluorescent protein: inhibition of migration and visualization of expression. Thromb Haemost 2000;84:460–7.
24. Saga Y, Mizukami H, Suzuki M, Urabe M, Kume A, Nakamura T, Sato I, Ozawa K. Expression of HGF/NK4 in ovarian cancer cells suppresses intraperitoneal dissemination and extends host survival. Gene Ther 2001;8:1450–5.
25. Kay MA, Manno CS, Ragni MV, Larson PJ, Couto LB, McClelland A, Glader B, Chew AJ, Tai SJ, Herzog RW, Arruda V, Johnson F, et al. Evidence for gene transfer and expression of factor IX in haemophilia B patients treated with an AAV vector. Nat Genet 2000;24: 257–61.
26. Ma HI, Guo P, Li J, Lin SZ, Chiang YH, Xiao X, Cheng SY. Suppression of intracranial human glioma growth after intramuscular administration of an adeno-associated viral vector expressing angiostatin. Cancer Res 2002;62:756–63.
27. Davidoff AM, Nathwani AC, Spurbeck WW, Ng CY, Zhou J, Vanin EF. rAAV-mediated long-term liver-generated expression of an angiogenesis inhibitor can restrict renal tumor growth in mice. Cancer Res 2002;62:3077–83.
28. Shimpo M, Ikeda U, Maeda Y, Takahashi M, Miyashita H, Mizukami H, Urabe M, Kume A, Takizawa T, Shibuya M, Ozawa K, Shimada K. AAV-mediated VEGF gene transfer into skeletal muscle stimulates angiogenesis and improves blood flow in a rat hindlimb ischemia model. Cardiovasc Res 2002;53:993–1001.

RESEARCH ARTICLE

Adeno-associated virus vector-mediated interleukin-10 gene transfer inhibits atherosclerosis in apolipoprotein E-deficient mice

T Yoshioka[1,2,3], T Okada[2], Y Maeda[1], U Ikeda[3], M Shimpo[1], T Nomoto[2], K Takeuchi[4], M Nonaka-Sarukawa[1], T Ito[1], M Takahashi[3], T Matsushita[2], H Mizukami[2], Y Hanazono[2], A Kume[2], S Ookawara[4], M Kawano[5], S Ishibashi[6], K Shimada[1] and K Ozawa[2]

[1]Division of Cardiovascular Medicine, Jichi Medical School, Tochigi, Japan; [2]Division of Genetic Therapeutics, Center for Molecular Medicine, Jichi Medical School, Tochigi, Japan; [3]Department of Organ Regeneration, Shinshu University Graduate School of Medicine, Matsumoto, Japan; [4]Department of Anatomy, Jichi Medical School, Tochigi, Japan; [5]Department of Laboratory Medicine, Jichi Medical School, Tochigi, Japan; and [6]Division of Endocrine and Metabolism, Jichi Medical School, Tochigi, Japan

Inflammation is a major contributor to atherosclerosis by its effects on arterial wall biology and lipoprotein metabolism. Interleukin-10 (IL-10) is an anti-inflammatory cytokine that may modulate the atherosclerotic disease process. We investigated the effects of adeno-associated virus (AAV) vector-mediated gene transfer of IL-10 on atherogenesis in apolipoprotein E (ApoE)-deficient mice. A murine myoblast cell line, C2C12, transduced with AAV encoding murine IL-10 (AAV2-mIL10) secreted substantial amounts of IL-10 into conditioned medium. The production of monocyte chemo-attractant protein-1 (MCP-1) by the murine macrophage cell line, J774, was significantly inhibited by conditioned medium from AAV2-mIL10-transduced C2C12 cells. ApoE-deficient mice were injected with AAV5-mIL10 into their anterior tibial muscle at 8 weeks of age. The expression of MCP-1 in the vascular wall of the ascending aorta and serum MCP-1 concentration were decreased in AAV5-mIL10-transduced mice compared with AAV5-LacZ-transduced mice. Oil red-O staining of the ascending aorta revealed that IL-10 gene transfer resulted in a 31% reduction in plaque surface area. Serum cholesterol concentrations were also significantly reduced in AAV5-mIL10-transduced mice. To understand the cholesterol-lowering mechanism of IL-10, we measured the cellular cholesterol level in HepG2 cells, resulting in its significant decrease by the addition of IL-10 in a dose-dependent manner. Furthermore, IL-10 suppressed HMG-CoA reductase expression in the HepG2 cells. These observations suggest that intramuscular injection of AAV5-mIL10 into ApoE-deficient mice inhibits atherogenesis through anti-inflammatory and cholesterol-lowering effects. Gene Therapy (2004) 11, 1772–1779. doi:10.1038/sj.gt.3302348; Published online 21 October 2004

Introduction

The inflammatory reaction involves complex interactions between inflammatory cells (lymphocytes and macrophages) and vascular endothelial and smooth muscle cells. The disturbance of vascular wall integrity and homeostasis by inflammation is thought to be a major contributor to atherosclerosis. Therefore, an anti-inflammatory strategy may be a promising approach to prevent and treat atherosclerotic disease. Another critical feature of atherogenesis is lipid accumulation. Several large-scale clinical trials have demonstrated that lipid reduction therapy involving HMG-CoA reductase inhibitor (statin) is useful for atherosclerotic disorders, such as ischemic heart disease.[1,2] Recent studies have indicated that statins have pleiotropic effects on the atherogenic process, including an anti-inflammatory effect.[3] On the

other hand, proinflammatory cytokines, such as tumor necrosis factor (TNF)-α, interleukin (IL)-1, and IL-6, have profound effects on lipid metabolism.[4] These findings suggest that there are complex interactions between inflammation and lipid metabolism.

IL-10, which is secreted by a wide variety of cells such as lymphocytes and macrophages, is a key inhibitor in a number of inflammatory responses,[5] including the production of proinflammatory cytokines and chemokines and the expression of endothelial adhesion molecules. IL-10 expression has been identified in early and advanced atherosclerotic plaques[6,7] and is thought to have potential antiatherogenic effects. Indeed, recent studies have shown that IL-10-transgenic mice fed a high-fat diet exhibit a decrease in atherogenesis.[8] Conversely, IL-10-deficient mice were found to suffer from more severe atherosclerosis, and the atherogenic tendency of these mice was ameliorated by the plasmid-mediated introduction of IL-10.[9] IL-10 is thought to have a protective role in human atherosclerotic disease as well.[10,11]

Despite the tremendous interest in the effects of cytokines on inflammation and lipoprotein metabolism, there have been few studies that have examined the

influence of IL-10 on these processes *in vivo*.[12,13] As atherogenesis is a chronic process, the long-term expression of IL-10 is required in order to assess its effects on this disease. In this study, we have used adeno-associated virus (AAV) vectors for IL-10 gene transfer to investigate the antiatherosclerotic effects of IL-10 *in vivo*, because these vectors can transduce skeletal muscle and permit the sustained expression and systemic delivery of therapeutic proteins following a single intramuscular administration.[14]

Results

IL-10 expression in C2C12 cells

We first verified the integrity of our vectors *in vitro*. Differentiated C2C12 cells, murine myoblasts, were transduced with AAV encoding murine IL-10 (AAV2-mIL10) at various dosages and cultured for 48 h. The concentration of IL-10 in the conditioned medium was found to increase in a vector dose-dependent manner (Figure 1a). Western blot analysis demonstrated the presence of an 18-kDa product, the size expected for murine IL-10, in the conditioned medium of AAV2-mIL10-transduced C2C12 cells, but not in the conditioned medium of AAV2-LacZ-transduced cells (Figure 1b).

To evaluate the biological activity of secreted IL-10, we examined the influence of conditioned medium from AAV2-mIL10-transduced C2C12 cells on cytokine production by J774 cells, murine macrophages. As shown in Figure 1c, treatment with lipopolysaccharide (LPS) increased the production of the cytokines, IL-6, TNF-α, and monocyte chemoattractant protein-1 (MCP-1), from J774 cells. These increases were significantly inhibited by the addition of conditioned medium from AAV2-mIL10-transduced C2C12 cells, and the production of these cytokines was completely restored in the presence of anti-mIL-10 antibody (1 μg/ml). Unstimulated J774 cells did not exhibit any change in cytokine expression when exposed to the conditioned medium.

IL-10 expression in apolipoprotein E-deficient mice

We next injected AAV2-mIL10 and AAV5-mIL10 into the anterior tibial muscle of apolipoprotein E (ApoE)-deficient mice. The serum concentration of IL-10 increased in a vector dose-dependent manner, and the efficacy of transduction was higher in AAV5-mIL10-treated mice than in AAV2-mIL10-treated mice at the same vector dose (1 × 10^13 genome copies/body) (Figure 2). When 1 × 10^12 genome copies/body of AAV5-mIL10 were injected, the serum IL-10 levels (1.2–4.9 ng/ml) were maintained at a higher than physiological range (up to 160 pg/ml) for 8 weeks. Moreover, the serum IL-10 levels at 14 months were 398.3 ± 146.6 pg/ml.

Effect of IL-10 on MCP-1 expression

We then investigated the anti-inflammatory effects of IL-10 in ApoE-deficient mice by focusing on the expression of MCP-1, a potent chemokine implicated in atherogenesis. ApoE-deficient mice transduced with AAV5-mIL10 at 4 weeks old were evaluated at 8 weeks old. Few atherosclerotic lesions were detected by oil red-O staining at this time point. An immunohistochemical analysis of MCP-1 in the aortic sinus of ApoE-deficient mice revealed that MCP-1 expression was modestly
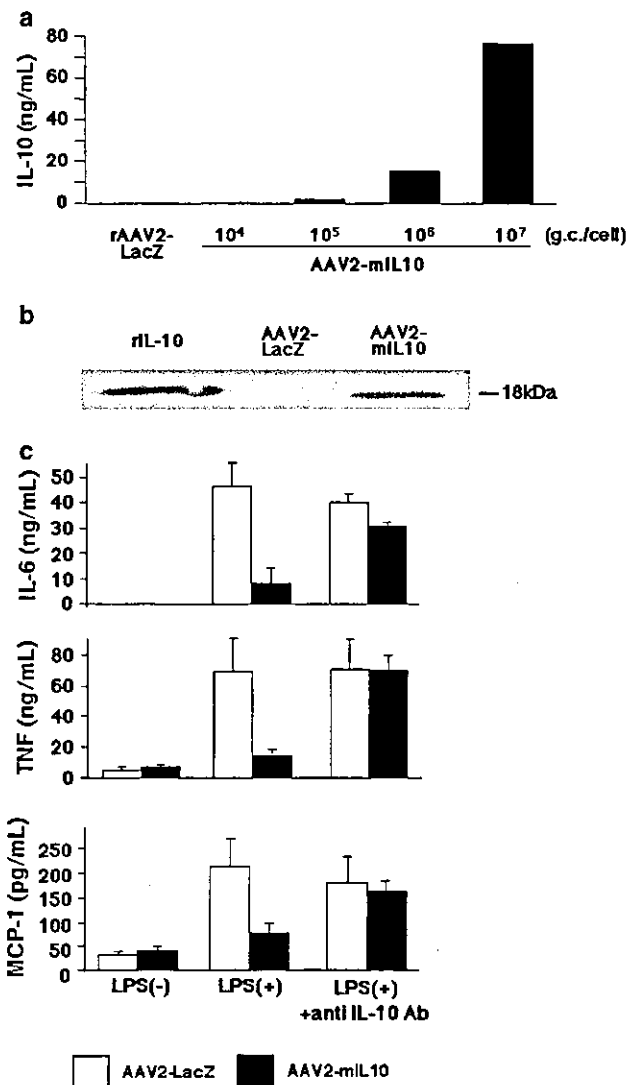

Figure 1 Transduction of the IL-10 gene into C2C12 cells with AAV2-mIL10. (a) Concentration of IL-10 in the conditioned medium of AAV2-mIL10-transduced C2C12 cells. The IL-10 concentration was measured by ELISA 48 h after transduction with the indicated number of genome copies per cell (g.c./cell). (b), Western blotting with an anti-IL-10 antibody was performed after immunoprecipitation of the conditioned medium of AAV2-mIL10- and AAV2-LacZ-transduced C2C12 cells. Recombinant mouse IL-10 (rIL-10) was used as a positive control. (c) LPS-stimulated J774 cells were incubated with the conditioned medium of AAV2-mIL10- (solid bars) or AAV2-LacZ (open bars)-transduced C2C12 cells for 24 h in the presence or absence of anti-IL-10 antibody (1 μg/ml). IL-6, TNF-α, and MCP-1 concentrations were analyzed by ELISA. Data are means ± s.e.m. (n = 4).

suppressed in AAV5-mIL10-transduced mice, whereas it was clearly observed in the vascular wall of AAV5-LacZ-transduced mice (Figure 3a). Moreover, 8 weeks after gene transfer, the serum concentration of MCP-1 in AAV5-mIL10-transduced mice was significantly reduced compared with that in AAV5-LacZ-transduced mice (Figure 3b).

Effects of IL-10 on atherogenesis

We evaluated the lesion area in ApoE-deficient mice fed an atherogenic diet 8 weeks after gene transfer. As shown in Figure 4, the aortic sinus of mice transduced with AAV5-mIL10 revealed a significant decrease in oil
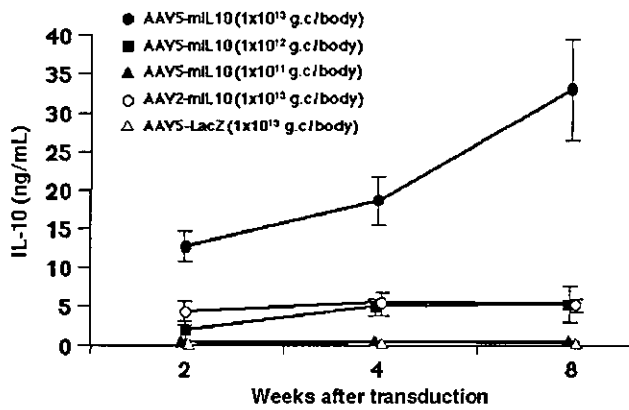
Figure 2 *Serum concentration of IL-10 after transduction of AAV-mIL10 into the anterior tibial muscle of ApoE-deficient mice. ApoE-deficient mice at 8 weeks of age were inoculated with AAV2-mIL10 (1×10^{13} g.c./body), AAV5-mIL10 ($1 \times 10^{11} \sim 1 \times 10^{13}$ g.c./body), or AAV5-LacZ (1×10^{13} g.c./body) by injection into the anterior tibial muscle. At 2, 4, and 8 weeks after injection, the serum IL-10 concentration was measured. Data are means ±s.e.m. (n = 3-7).*
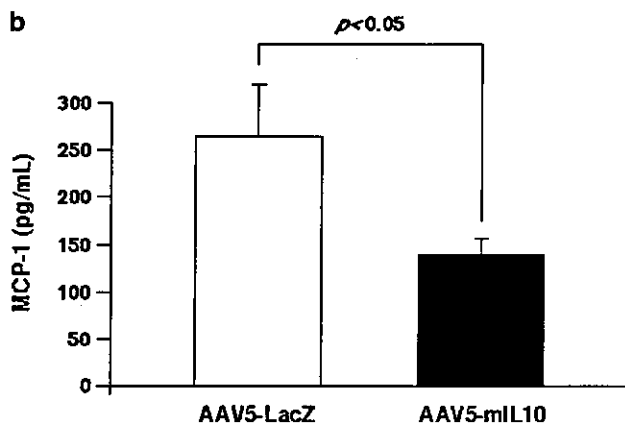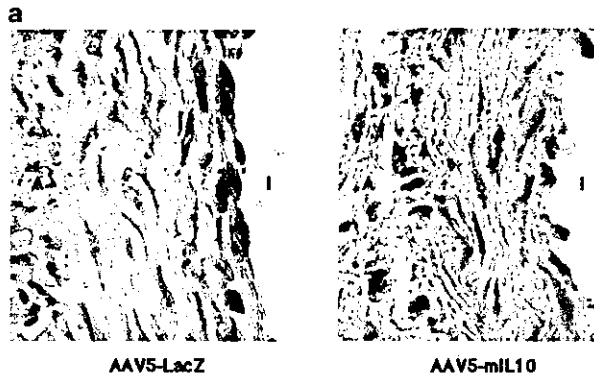

Figure 3 *Systemic and local MCP-1 expression in ApoE-deficient mice. (a) Immunohistochemical staining of the aortic sinus segment in ApoE-deficient mice was performed 4 weeks after inoculation with AAV5-mIL10 (1×10^{12} g.c./body). Enhanced MCP-1 expression was observed in the vascular wall of AAV5-LacZ mice, but was suppressed in AAV5-mIL10-transduced mice. I, intima; A, adventitia. (b) The serum MCP-1 concentration in ApoE-deficient mice was measured 8 weeks after inoculation with AAV5-mIL10 or AAV5-LacZ. Means and s.e.m. for each group are presented as histograms (n = 6 for LacZ, n = 13 for IL-10).*

Figure 4 *The inhibitory effect of IL-10 on atherogenesis in ApoE-deficient mice. (a) At 8 weeks after inoculation with AAV5-mIL10 (1×10^{12} g.c./body), the proximal aortas were removed, sectioned, and stained with oil red-O. (b) Oil red-O-positive areas were analyzed in comparison with the total cross-sectional vessel wall area. The average values for five sites from each animal were used for analysis. Means and s.e.m. for each group are presented as histograms (n = 5 for LacZ, n = 9 for IL-10).*

(AAV5-IL-10, $26.5 \pm 1.9\%$ *versus* AAV5-LacZ, $37.7 \pm 2.2\%$ of total cross-sectional vessel wall area, $P < 0.01$). Figure 5 shows that serum MCP-1 concentration correlates with the extent of atherosclerotic lesion formation, suggesting that a decrease in MCP-1 expression is related to a decrease in atherosclerotic lesion formation.

Effect of IL-10 on lipids

We investigated the effects of IL-10 expression on the level of serum lipids. Total cholesterol levels were significantly reduced in the AAV5-mIL10-transduced mice (931 ± 432, 1074 ± 419 mg/dl) compared to the AAV5-LacZ-transduced mice (2212 ± 640, 1840 ± 421 mg/dl, 4 weeks and 8 weeks after gene transfer, respectively). Triglyceride level in the AAV5-IL10-transduced mice 8 weeks after gene transfer was also reduced (171.7 ± 67.3 mg/dl) compared to that in the AAV5-LacZ-transduced mice (291.6 ± 172.4 mg/dl, $P < 0.05$).

Nonlinear regression fitting to a sigmoidal dose curve revealed a high correlation between the serum cholesterol level and IL-10 concentration ($r = 0.857$), with an estimated EC_{50} of 5.3 ng/ml (Figure 6a). In addition, the serum cholesterol concentration positively correlated with the atherosclerotic lesion area ($r = 0.728$, $P < 0.01$; Figure 6b). IL-10 gene transfer did not affect body

red-O-positive areas compared to that of mice transduced with AAV5-LacZ. The systemic overexpression of IL-10 resulted in a 31% reduction in plaque surface area
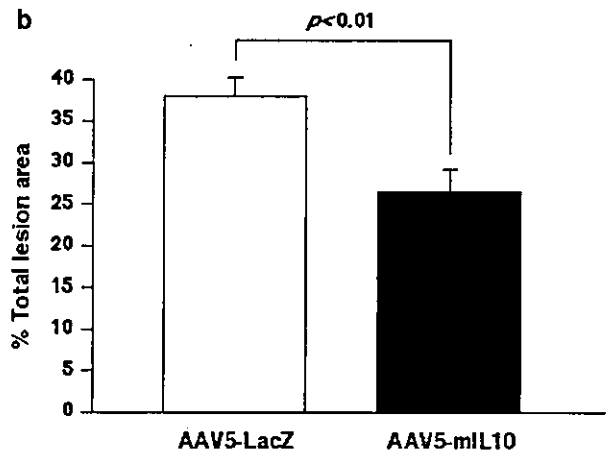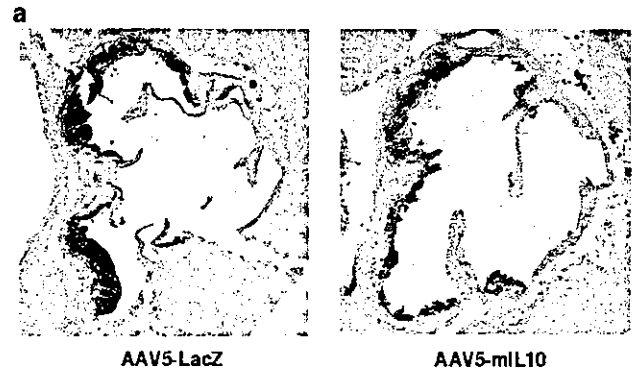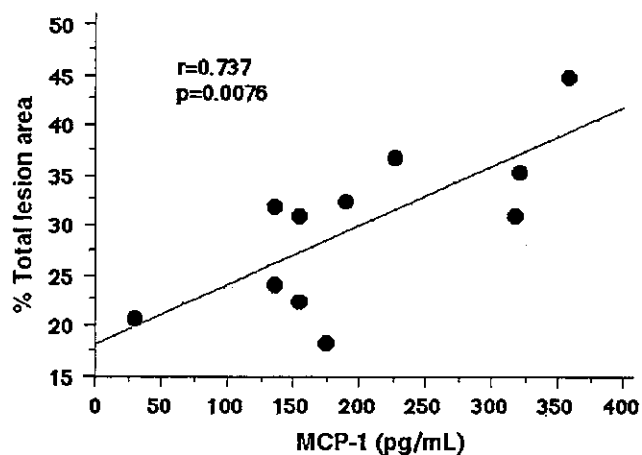
Figure 5 Correlation between serum MCP-1 concentration and extent of atherosclerotic lesion formation. The serum MCP-1 concentration positively correlated with oil red-O-positive surface area in ApoE-deficient mice 8 weeks after inoculation with AAV5-mIL10 (r = 0.737, P = 0.0076).

weight, food intake, blood sugar levels, or blood pressure (data not shown).

To assess whether IL-10 causes changes in the lipoprotein profile of apoE-deficient mice, plasma lipoproteins were subjected to agarose gel electrophoresis. No differences in the patterns of lipoprotein expression were observed in AAV5-mIL10-transduced mice and AAV5-LacZ-transduced mice (data not shown).

To further understand the mechanism by which the serum cholesterol level is decreased in AAV5-mIL10-transduced mice, we evaluated cholesterol levels of HepG2 cells, human hepatocytes, incubated in the absence of lipoprotein. As shown in Figure 7, the level of cholesterol in HepG2 cells was significantly decreased by the addition of IL-10 in a dose-dependent manner. The level of intracellular cholesterol was also significantly decreased by the addition of HMG-CoA reductase inhibitor, fluvastatin, to these cells. When HepG2 cells were incubated in the presence of lipoprotein, the level of cholesterol in the conditioned medium was not decreased by the addition of IL-10 (data not shown). These data suggest that IL-10 reduces *de novo* cholesterol synthesis, but does not stimulate cholesterol uptake by hepatocytes. Furthermore, we estimated the effect of IL-10 on the expression of HMG-CoA reductase. Interestingly, IL-10 significantly decreased mRNA levels of HMG-CoA reductase $(P < 0.01)$, while fluvastatin, enzyme inhibitor, did not alter the expression of the enzyme itself (Figure 8).

Discussion

IL-10, a pleiotropic cytokine produced by Th2-type T cells, B cells, monocytes, and macrophages, has potent anti-inflammatory properties. The main finding of the present study is that AAV vector-mediated IL-10 gene transfer to ApoE-deficient mice following a single intramuscular administration inhibits atherosclerotic lesion formation through the inhibition of MCP-1 expression and the reduction in the level of serum cholesterol.
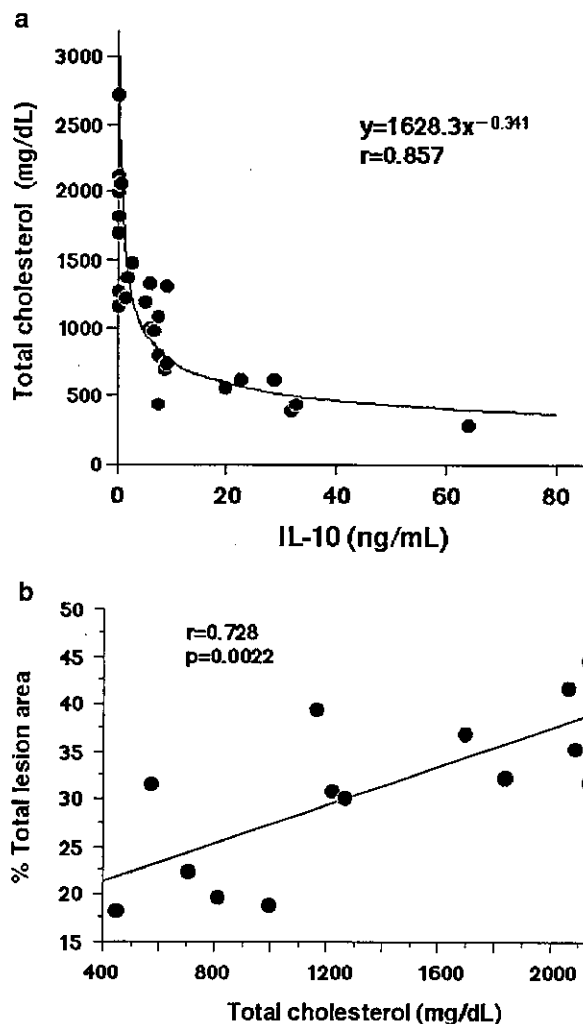

Figure 6 (a) Curve-fitting of the serum cholesterol concentration against the serum IL-10 concentration 8 weeks after inoculation of AAV5-mIL10 yielded a close fit (r = 0.857) to a dose–response curve $(y = 1628.3 \times ^{-0.341})$, with an EC_{50} of 5.3 ng/ml. (b) The serum cholesterol level positively correlated with atherosclerotic lesion surface area 8 weeks after inoculation with AAV5-mIL10 (r = 0.728, P = 0.0022).

Differentiated C2C12 cells transduced with AAV2-mIL10 were verified by Western blot analysis and enzyme-linked immunosorbent assay (ELISA) to express IL-10. The biological activity of the secreted IL-10 was also confirmed. Conditioned medium from C2C12 cells transduced with AAV2-mIL10 significantly inhibited the production of IL-6, TNF-α, and MCP-1 by J774 cells in response to LPS treatment. Based on these *in vitro* observations, we used recombinant AAV constructs to evaluate the effects of IL-10 on atherogenesis in ApoE-deficient mice. Intramuscular injection of AAV5-mIL10 into ApoE-deficient mice resulted in long-term systemic IL-10 expression. The serum IL-10 concentration was sustained at levels higher than 398.3 ± 146.6 pg/ml $(n = 6)$ up to 14 months after gene transfer $(1 \times 10^{12}$ genome copies/body).

Although double-stranded AAV genomes probably remain extrachromosomal in mouse myofibers, their tight association with chromatin allows their persistence and stable expression over periods of several months.[15–17] This particular feature of AAV vectors might be advanta-
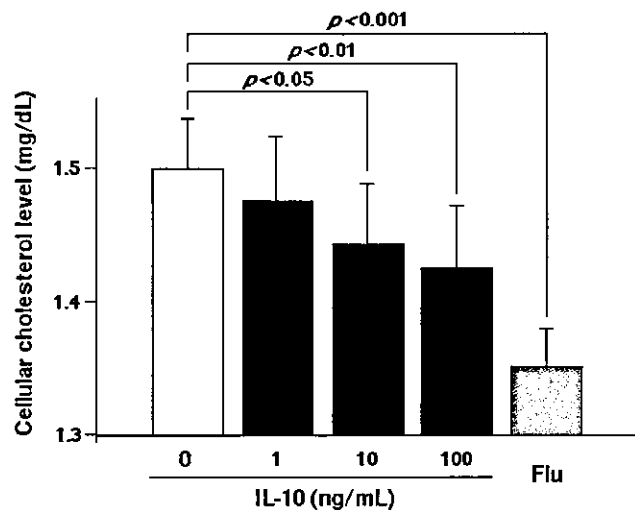
Figure 7 Cellular cholesterol level of HepG2 cells incubated in the absence of LDL cholesterol. Recombinant human IL-10 (1–100 ng/ml) or fluvastatin (10^{-5} mol/l) was added to the culture for 48 h. Data are means ± s.e.m. (n = 4).
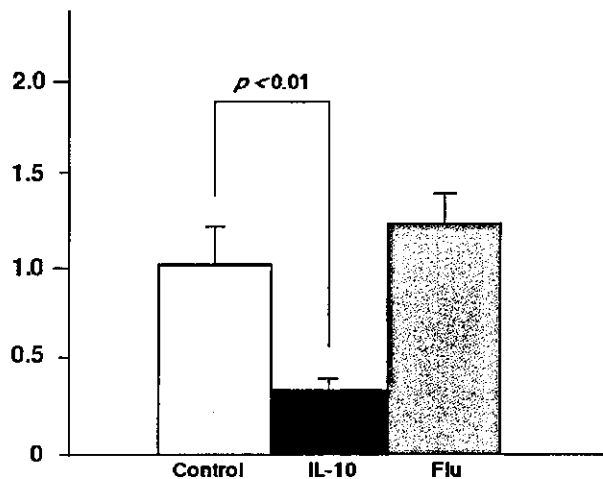

Figure 8 Relative HMG-CoA reductase expression in HepG2 treated with recombinant IL-10 as analyzed by quantitative PCR. The relative expression of the HMG-CoA reductase mRNA was determined as the ratio of the expression in HepG2 treated with IL-10 or fluvastatin to that in HepG2 incubated normally (control). Data are means ± s.e.m. (n = 3–5).

geous in investigating the effects of transgenes on chronic disease processes. Previous reports demonstrated that there was a significant difference in transgene expression by various AAV serotypes transduced into rodent muscle.[18-20] The AAV1 and AAV5 serotypes were shown to produce 100- to 1000-fold higher serum levels of transgene products, as compared to the AAV2. We selected AAV5 for use in in vivo experiments, since we also observed that gene transfer with AAV5 promoted a much higher level of expression of IL-10, as compared to AAV2-mediated transfer (Figure 2). However, AAV1 is reported to more efficiently transduce muscle than AAV5. Therefore, we anticipate that the use of AAV1 in future experiments would allow for a minimized vector dosage.

We focused on the effect of IL-10 on in vivo MCP-1 expression. MCP-1, one of the most studied members of the C–C family of chemokines, is expressed in several cell types in the arterial wall, including vascular

endothelial cells, smooth muscle cells, and monocytes/ macrophages, under numerous inflammatory conditions. Therefore, MCP-1 is thought to play an important role in the ongoing recruitment of monocyte–macrophages into developing lesions in vivo.[21] Previously, we[22] and others[21,23] reported enhanced MCP-1 expression in experimental and human atherosclerotic lesions. A role for MCP-1 in the initiation of atherogenesis was demonstrated by knockout mice in which the MCP-1 gene itself or its receptor CCR2 was inactivated.[24,25] In our study, we demonstrated that serum MCP-1 concentrations are significantly lower in IL-10-transduced mice than in control mice. In addition, we observed enhanced MCP-1 expression in the vascular wall of ApoE-deficient mice, as reported previously,[26] which was significantly inhibited by IL-10 gene transfer. Moreover, the extent of atherosclerotic lesion formation was significantly decreased in AAV5-mIL10-transduced mice, and positively correlated with serum MCP-1 concentration. These results suggest that the observed antiatherogenic effect of IL-10 is partly mediated by the inhibition of systemic and local MCP-1 expression.

We also investigated the effect of IL-10 on serum cholesterol levels. Nonlinear regression of serum cholesterol levels relative to serum IL-10 levels revealed a close correlation to a dose–effect model with an EC_{50} (5.3 ng/ ml). It is well known that high cholesterol levels lead to atherogenesis in both humans and mice. Atherosclerotic lesion surface area also correlated with the serum cholesterol concentration in our study. van Exel et al[12] recently found a negative correlation between a low IL-10 production capacity of whole blood and total cholesterol level in humans. They speculated that high levels of IL-10 counteract the effects of TNF-α and IL-6 on lipid metabolism. This clinical observation corresponds well with our observation that the serum IL-10 concentration negatively correlates with the reduction in serum cholesterol.

Pinderski et al[8] found that IL-10-transgenic mice showed a decrease in atherosclerotic lesions compared to control mice. However, they found no difference in plasma cholesterol levels between the transgenic and control mice. On the other hand, Von Der Thusen et al[13] showed that prolonged hepatic expression of IL-10 could be achieved following intravenous adenovirus-mediated IL-10 gene transfer to LDL receptor-deficient mice. Administration of IL-10 resulted in reductions in atherosclerotic lumen stenosis and of serum cholesterol, although the cholesterol-lowering mechanism was not clarified.

We analyzed the intracellular cholesterol level of HepG2 cells cultured with acetic acid, a cholesterol substrate, in the absence of lipoprotein. This assay can measure de novo cholesterol synthesis, but not cholesterol uptake, in these cells. We also used fluvastatin at a dose of 10^{-5} mol/l to inhibit de novo cholesterol synthesis almost completely.[27] The results of these experiments suggested that IL-10, like fluvastatin, significantly inhibits the hepatic production of cholesterol. It was reported that TNF-α and IL-1 increase the levels of HMG-CoA reductase mRNA without affecting the levels of LDL receptor mRNA.[28] In other words, the increase in serum cholesterol levels observed after TNF-α and IL-1 administration is caused by an increase in hepatic cholesterol synthesis rather than a decrease in the

clearance of circulating cholesterol. These observations suggest that IL-10 might have direct effects on cholesterol metabolism through the HMG-CoA reductase pathway. We evaluated the expression of HMG-CoA reductase using quantitative PCR. As is expected, IL-10 modulated HMG-CoA reductase expression, whereas fluvastatin did not. These data suggest that the use of IL-10 in combination with statin may improve cholesterol-lowering effects and benefit the patients with atherosclerotic diseases.

Finally, we evaluated whether the downregulation of the MCP-1 was affected by the cholesterol-lowering effects of IL-10 or not. Stepwise regression analysis revealed that not only serum cholesterol but also MCP-1 concentration might be significant independent predictors of atherosclerotic lesion area. Therefore, we speculated that anti-inflammatory effect of IL-10 plays an important role in anti-atherogenic effect as well as its cholesterol-lowering effects.

In summary, AAV5-mediated IL-10-gene transfer into the skeletal muscle could introduce efficient and stable IL-10 expression, resulting in a significant antiatherogenic effects in ApoE-deficient mice. It was suggested that this effect was mediated through the anti-inflammatory and cholesterol-lowering effects of IL-10. These results indicate the presence of complex interactions between inflammation and lipid metabolism, as well as the effectiveness of anticytokine therapy using IL-10 in the treatment of atherosclerotic disease.

Materials and methods

Production of AAV vectors

Two recombinant AAV serotypes, type 2 and type 5, were used in these experiments. AAV2 and AAV5 expressing the *Escherichia coli* β-galactosidase gene under the control of the cytomegalovirus promoter (AAV2-LacZ and AAV5-LacZ) were generated with the proviral plasmids pAAV-LacZ and pAAV5-RNL, respectively. To create AAV2 and AAV5 derivatives expressing murine IL-10 (AAV2-mIL10 and AAV5-mIL10), murine IL-10 cDNA (RIKEN DNA Bank, RDB-1476) was cloned into the *Bam*HI site of pCMV to form pCMVmIL10. The IL-10 expression cassette in pCMVmIL10 was ligated as a *Not*I fragment to *Not*I-digested pAAV-LacZ and pAAV5-RNL to form the proviral plasmids pAAV2-mIL10 and pAAV5-mIL10, respectively.

AAV viral stocks were prepared according to the previously described three-plasmid transfection adenovirus-free protocol.[29] Briefly, 60% confluent 293 cells were cotransfected with the proviral plasmid, an AAV helper plasmid (pHLP19[30] for AAV2 or pAAV5RepCap[31] for AAV5), and the adenoviral helper plasmid pAdeno. The crude viral lysate was purified by two rounds of CsCl two-tier centrifugation.[32] The viral stock was titered by dot-blot hybridization with plasmid standards.

pAAV5-RNL and pAAV5-RepCap (identical to 5RepCapB) were kindly provided by Dr JA Chiorini, and pAAV-LacZ, pHLP19 and pAdeno were obtained from Avigen, Inc. (Alameda, CA, USA).

In vitro IL-10 gene transfer

The C2C12 cells were cultured in six-well plates with 2 ml Dulbecco's minimal essential medium (DMEM) containing 5% horse serum. At 8 days after plating, differentiated C2C12 cells were transduced with AAV2-mIL10 at various vector doses. The expression of IL-10 was detected by Western blot analysis after immunoprecipitation of conditioned medium and cell lysates. IL-10 concentrations were measured by ELISA (R&D Systems). To investigate the biological activities of IL-10, cultured medium from transduced C2C12 cells was added to cultured J774 cells for 30 min (final IL-10 concentration, 10 ng/ml). J774 cells were then treated with 100 ng/ml LPS and incubated for an additional 24 h. The supernatants were harvested and the concentrations of IL-6, TNF-α, and MCP-1 were quantified by ELISA (R&D Systems).

In vivo IL-10 gene transfer

All animal experiments were performed in accordance with the *Jichi Medical School Guide for Laboratory Animals*, 1993. Male ApoE-deficient mice in the C57BL/6J background (a kind gift of Dr N Maeda[33,34]) were fed on a Western-type diet containing 21% fat and 0.15% cholesterol (Harlan Teklad) from 8 weeks of age. Water and food were given *ad libitum*, and the mice were maintained on a 12-h light–dark cycle. At 8 weeks of age, ApoE-deficient mice were injected with AAV2-mIL10 (1×10^{13} genome copies/body), AAV5-mIL10 (1×10^{11}–10^{13} genome copies/body), or AAV5-LacZ (1×10^{13} genome copies/body) as 50 μl in total into two distinct sites of the anterior tibial muscle. The serum concentrations of IL-10 and MCP-1 were measured by ELISA as described above. The serum concentrations of total cholesterol were measured by HDAOS methods (Wako Pure Chemicals).

Morphometric analysis

At 8 weeks after the AAV5-mIL10 or -LacZ inoculation, the ascending aortas were removed after perfusion fixation with 4% paraformaldehyde at physiological pressure, embedded in OCT compound (Tissue-Tek), and frozen in liquid nitrogen. Atherosclerotic lesions in the aortic sinus were examined at five locations separated by 80 μm, with the most proximal site at the point where the aortic valves first appeared, and were stained with oil red-O. To quantify the aortic lesions, each image was digitized and analyzed under a microscope (Olympus) with National Institutes of Health Image software (ver. 1.61). Oil red-O-positive areas were analyzed in comparison with the total cross-sectional vessel wall area. The average value for five locations in each animal was determined.

Immunohistochemical analysis

Arterial sections were prepared from 8-week-old mice transduced with AAV5-IL-10 or AAV5-LacZ at 4 weeks old. These sections were incubated with a primary goat polyclonal antibody against mouse MCP-1 (dilution 1/250, Santa Cruz Biotechnology). Nonspecific IgG was used as a negative control. Sections were incubated with biotinylated anti-mouse secondary antibody and treated with peroxidase-conjugated streptavidin, with 3′, 3′-diaminobenzidine tetrahydrochloride as the enzyme substrate, and counterstained with hematoxylin.

Measurement of cellular cholesterol

HepG2 cells (human hepatocytes) were maintained in a 12-well plate with 1 ml of MEM containing 10% fetal bovine serum, 1% nonessential amino acids (NEAA; ICN), and 1 mmol/l sodium pyruvate at 37°C in a 5% CO_2 incubator for 5 days. The medium was then replaced with 1 ml of MEM containing 10% lipoprotein-deficient serum (LPDS; ICN), 1% NEAA, and 1 mmol/l sodium pyruvate. After 2 days later, the cells were incubated with 1 ml of MEM containing 10% LPDS, 1% NEAA and 1 mmol/l sodium pyruvate, and various concentrations (0–100 ng/ml) of recombinant human IL-10 (PeproTech) or 10^{-5} mol/l fluvastatin (Tanabe) were added to the culture. At 2 days after the treatment, the cells were incubated with 0.5 ml of MEM containing 10% LPDS, 1% NEAA, 1 mmol/l sodium pyruvate, and 2 mmol/l acetic acid for 16 h. The cellular cholesterol level was measured by an enzymatic method using Determiner TC-555 (Kyowa Medics).

mRNA analysis of HMG-CoA reductase

HepG2 cells were incubated with either recombinant human IL-10 (10 ng/ml) or fluvastatin (10^{-5} mol/l) in 10% LPDS medium for 24 h. Total RNA was isolated from the cell culture using an RNeasy Mini kit (QIAGEN) and reverse-transcribed into a single-stranded cDNA using SuperScript Preamplification System (GIBCO BRL). To estimate the expression of HMG-CoA reductase in HepG2, quantitative PCR analysis was conducted by using ABI PRISM 7700 Sequence Detection System (Applied Biosystems). The reaction was performed using the primer pairs specific for the *HMG-CoA reductase* (HMGCR-5': GGCCCA GTTGTGCGTCTTCC and HMGCR-3': GTTTGCTGC ATGGGCGTTGTAG) and *GAPDH* (GAPDH-5': CGCG GGGCTCTCCAGAACATCAT and GAPDH-3': CCAGCC CCAGCGTCAAAGGTG). Quantitative values were obtained from the threshold cycle (C_t) number that indicated exponential amplification of the PCR product. To normalize each sample, we also quantified the expression of the *GAPDH* gene. The relative target gene expression was also normalized with a calibrator (HepG2 cells without treatment of IL-10 or fluvastatin). The final result, expressed as *N*-fold differences in target gene expression relative to the *GAPDH* gene and the calibrator, was determined by the following formula: $N_{target} = 2^{correctedΔC_t\,(GAPDH-target\,gene)}$. C_t values of the sample were determined by subtracting the average C_t value of the target gene from the average C_t value of the *GAPDH* gene.

Statistical analysis

Student's *t*-test or ANOVA combined with Scheffe's test was used to compare individual groups, and the Pearson's correlation test was employed to measure the linear association between two variables by using StatView (Abacus Concepts, Inc). Data are presented as means ± s.e.m. A value of $P < 0.05$ was considered significant.

Acknowledgements

References

1 The Scandinavian Simvastatin Survival Study Group. Randomised trial of cholesterol lowering in 4444 patients with coronary heart disease: the Scandinavian Simvastatin Survival Study (4S). *Lancet* 1994; 344: 1383–1389.

2 Shepherd J et al. Prevention of coronary heart disease with pravastatin in men with hypercholesterolemia. West of Scotland Coronary Prevention Study Group. *N Engl J Med* 1995; 333: 1301–1307.

3 Chen H, Ikeda U, Shimpo M, Shimada K. Direct effects of statins on cells primarily involved in atherosclerosis. *Hypertens Res* 2000; 23: 187–192.

4 Feingold KR, Grunfeld C. Role of cytokines in inducing hyperlipidemia. *Diabetes* 1992; 41 (Suppl 2): 97–101.

5 Fiorentino DF, Bond MW, Mosmann TR. Two types of mouse T helper cell. IV. Th2 clones secrete a factor that inhibits cytokine production by Th1 clones. *J Exp Med* 1989; 170: 2081–2095.

6 Uyemura K et al. Cross-regulatory roles of interleukin (IL)-12 and IL-10 in atherosclerosis. *J Clin Invest* 1996; 97: 2130–2138.

7 Mallat Z et al. Expression of interleukin-10 in advanced human atherosclerotic plaques: relation to inducible nitric oxide synthase expression and cell death. *Arterioscler Thromb Vasc Biol* 1999; 19: 611–616.

8 Pinderski Oslund LJ et al. Interleukin-10 blocks atherosclerotic events *in vitro* and *in vivo*. *Arterioscler Thromb Vasc Biol* 1999; 19: 2847–2853.

9 Mallat Z et al. Protective role of interleukin-10 in atherosclerosis. *Circ Res* 1999; 85: e17–e24.

10 Smith DA et al. Serum levels of the antiinflammatory cytokine interleukin-10 are decreased in patients with unstable angina. *Circulation* 2001; 104: 746–749.

11 Anguera I et al. Elevation of serum levels of the anti-inflammatory cytokine interleukin-10 and decreased risk of coronary events in patients with unstable angina. *Am Heart J* 2002; 144: 811–817.

12 van Exel E et al. Low production capacity of interleukin-10 associates with the metabolic syndrome and type 2 diabetes: the Leiden 85-Plus study. *Diabetes* 2002; 51: 1088–1092.

13 Von Der Thusen JH et al. Attenuation of atherogenesis by systemic and local adenovirus-mediated gene transfer of interleukin-10 in LDLr−/− mice. *FASEB J* 2001; 15: 2730–2732.

14 Kessler PD et al. Gene delivery to skeletal muscle results in sustained expression and systemic delivery of a therapeutic protein. *Proc Natl Acad Sci USA* 1996; 93: 14082–14087.

15 Duan D et al. Circular intermediates of recombinant adeno-associated virus have defined structural characteristics responsible for long-term episomal persistence in muscle tissue. *J Virol* 1998; 72: 8568–8577.

16 Bohl D et al. Improvement of erythropoiesis in beta-thalassemic mice by continuous erythropoietin delivery from muscle. *Blood* 2000; 95: 2793–2798.

17 Shimpo M et al. AAV-mediated VEGF gene transfer into skeletal muscle stimulates angiogenesis and improves blood flow in a rat hindlimb ischemia model. *Cardiovasc Res* 2002; 53: 993–1001.

18 Chao H et al. Several log increase in therapeutic transgene delivery by distinct adeno-associated viral serotype vectors. Mol Ther 2000; 2: 619–623.

19 Duan D et al. Enhancement of muscle gene delivery with pseudotyped adeno-associated virus type 5 correlates with myoblast differentiation. J Virol 2001; 75: 7662–7671.

20 Rabinowitz JE et al. Cross-packaging of a single adeno-associated virus (AAV) type 2 vector genome into multiple AAV serotypes enables transduction with broad specificity. J Virol 2002; 76: 791–801.

21 Yla-Herttuala S et al. Expression of monocyte chemoattractant protein 1 in macrophage-rich areas of human and rabbit atherosclerotic lesions. Proc Natl Acad Sci USA 1991; 88: 5252–5256.

22 Seino Y et al. Expression of monocyte chemoattractant protein-1 in vascular tissue. Cytokine 1995; 7: 575–579.

23 Nelken NA, Coughlin SR, Gordon D, Wilcox JN. Monocyte chemoattractant protein-1 in human atheromatous plaques. J Clin Invest 1991; 88: 1121–1127.

24 Gu L et al. Absence of monocyte chemoattractant protein-1 reduces atherosclerosis in low density lipoprotein receptor-deficient mice. Mol Cell 1998; 2: 275–281.

25 Boring L, Gosling J, Cleary M, Charo IF. Decreased lesion formation in CCR2−/− mice reveals a role for chemokines in the initiation of atherosclerosis. Nature 1998; 394: 894–897.

26 Rayner K, Van Eersel S, Groot PH, Reape TJ. Localisation of mRNA for JE/MCP-1 and its receptor CCR2 in atherosclerotic lesions of the ApoE knockout mouse. J Vasc Res 2000; 37: 93–102.

27 Mascaro C et al. Sterol regulatory element binding protein-mediated effect of fluvastatin on cytosolic 3-hydroxy-3-methylglutaryl-coenzyme A synthase transcription. Arch Biochem Biophys 2000; 374: 286–292.

28 Hardardottir I et al. Effects of TNF, IL-1, and the combination of both cytokines on cholesterol metabolism in Syrian hamsters. Lymphokine Cytokine Res 1994; 13: 161–166.

29 Matsushita T et al. Adeno-associated virus vectors can be efficiently produced without helper virus. Gene Therapy 1998; 5: 938–945.

30 Okada T et al. Development and characterization of an antisense-mediated prepackaging cell line for adeno-associated virus vector production. Biochem Biophys Res Commun 2001; 288: 62–68.

31 Chiorini JA, Kim F, Yang L, Kotin RM. Cloning and characterization of adeno-associated virus type 5. J Virol 1999; 73: 1309–1319.

32 Okada T et al. Adeno-associated viral vector-mediated gene therapy of ischemia-induced neuronal death. Methods Enzymol 2002; 346: 378–393.

33 Zhang SH, Reddick RL, Piedrahita JA, Maeda N. Spontaneous hypercholesterolemia and arterial lesions in mice lacking apolipoprotein E. Science 1992; 258: 468–471.

34 Ishibashi S et al. The two-receptor model of lipoprotein clearance: tests of the hypothesis in "knockout" mice lacking the low density lipoprotein receptor, apolipoprotein E, or both proteins. Proc Natl Acad Sci USA 1994; 91: 4431–4435.

High-Level *in Vivo* Gene Marking after Gene-Modified Autologous Hematopoietic Stem Cell Transplantation without Marrow Conditioning in Nonhuman Primates

Kyoji Ueda,[1,2] Yutaka Hanazono,[1,*] Hiroaki Shibata,[1,3] Naohide Ageyama,[3] Yasuji Ueda,[4] Satoko Ogata,[1,4] Toshiaki Tabata,[4] Takeyuki Nagashima,[4] Masaaki Takatoku,[6] Akihiko Kume,[1] Susumu Ikehara,[5] Masafumi Taniwaki,[2] Keiji Terao,[3] Mamoru Hasegawa,[4] and Keiya Ozawa[1,6,*]

[1] Center for Molecular Medicine and [6] Division of Hematology, Department of Medicine, Jichi Medical School, Tochigi 329-0498, Japan
[3] Tsukuba Primate Center, National Institute of Infectious Diseases, Ibaraki 305-0843, Japan
[4] DNAVEC Corporation, Ibaraki 305-0856, Japan
[5] First Department of Pathology, Kansai Medical University, Osaka 570-8506, Japan
[2] Division of Hematology and Oncology, Department of Medicine, Kyoto Prefectural University of Medicine, Kyoto 602-8566, Japan

*To whom correspondence and reprint requests should be addressed at the Center for Molecular Medicine, Jichi Medical School, 3311-1 Yakushiji, Minamikawachi, Tochigi 329-0498, Japan. Fax: +81-285-44-5205. E-mail: hanazono@jichi.ac.jp.

The successful engraftment of genetically modified hematopoietic stem cells (HSCs) without toxic conditioning is a desired goal for HSC gene therapy. To this end, we have examined the combination of intrabone marrow transplantation (iBMT) and *in vivo* expansion by a selective amplifier gene (SAG) in a nonhuman primate model. The SAG is a chimeric gene consisting of the erythropoietin (EPO) receptor gene (as a molecular switch) and c-Mpl gene (as a signal generator). Cynomolgus CD34$^+$ cells were retrovirally transduced with or without SAG and returned into the femur and humerus following irrigation with saline without prior conditioning. After iBMT without SAG, 2–30% of colony-forming cells were gene marked over 1 year. The marking levels in the peripheral blood, however, remained low (<0.1%). These results indicate that transplanted cells can engraft without conditioning after iBMT, but *in vivo* expansion is limited. On the other hand, after iBMT with SAG, the peripheral marking levels increased more than 20-fold (up to 8–9%) in response to EPO even at 1 year posttransplant. The increase was EPO-dependent, multilineage, polyclonal, and repeatable. Our results suggest that the combination of iBMT and SAG allows efficient *in vivo* gene transduction without marrow conditioning.

Key Words: gene therapy, hematopoietic stem cell, intrabone marrow transplantation, nonconditioning, *in vivo* expansion, selective amplifier gene, nonhuman primate

INTRODUCTION

The ability to expand selectively cells containing potentially therapeutic genes *in vivo* would represent an important tool for the clinical application of hematopoietic stem cell (HSC)-based gene transfer. This would circumvent low gene transfer efficiency into HSCs, which is one of the current limitations of this promising technology. Furthermore, the ability to expand genetically modified cells *in vivo* would circumvent another major problem of HSC gene therapy; myeloablative conditioning is necessary unless gene-modified cells have clear growth advan-

tage [1]. Current myeloablative conditioning regimens are associated with high systemic toxicity and potential damage to marrow stroma, possibly resulting in impaired engraftment [2]. With the *in vivo* selection method using a drug-resistance gene, engraftment of transduced cells at low levels may allow successful expansion to clinically relevant levels even without marrow conditioning, although the administration of cytotoxic agents is required for the selection [3]. It has recently been reported that bone marrow cells can efficiently engraft mice without marrow conditioning when implanted directly into the

469

bone marrow cavity (intrabone marrow transplantation, iBMT) [4,5]. Using the iBMT method, human cord blood cells are also able to engraft efficiently in bone marrow of sublethally irradiated immunodeficient mice [6–8]. Although the iBMT method has been successful in mice, the efficacy in primates remains to be examined.

.We have previously developed a selective amplifier gene (SAG) consisting of a chimeric gene encoding the granulocyte colony-stimulating factor (G-CSF) receptor (as a growth-signal generator) and the hormone-binding domain of the steroid receptor (as a molecular switch) [9]. Hematopoietic cells genetically engineered to express this SAG can be expanded in a steroid-dependent manner *in vitro* and *in vivo* in mice and nonhuman primates [10,11]. Here we have examined such expansion in the setting of nonhuman primate iBMT without marrow conditioning using a new SAG encoding the erythropoietin (EPO) receptor (as a molecular switch) and thrombopoietin receptor (c-Mpl; as a signal generator) [12].

RESULTS

Engraftment after iBMT

First, we examined whether gene-marked CD34^{+} cells engraft after iBMT using two cynomolgus macaques. Cynomolgus CD34^{+} cells were transduced with the nonexpression retroviral vector PLI (which contains untranslated sequence) [13]. The transduction results are summarized in Table 1. We injected the transduced CD34^{+} cells directly into the bone marrow cavity of four proximal limb bones (the femurs and humeri) after gently irrigating the cavity with saline (Fig. 1). This transplant procedure was safely performed without pulmonary embolism or infection of bone marrow. Conditioning treatment such as irradiation was not conducted prior to transplantation. In addition, we returned the transduced CD34^{+} cells into two monkeys by the conventional transplantation method without prior conditioning.
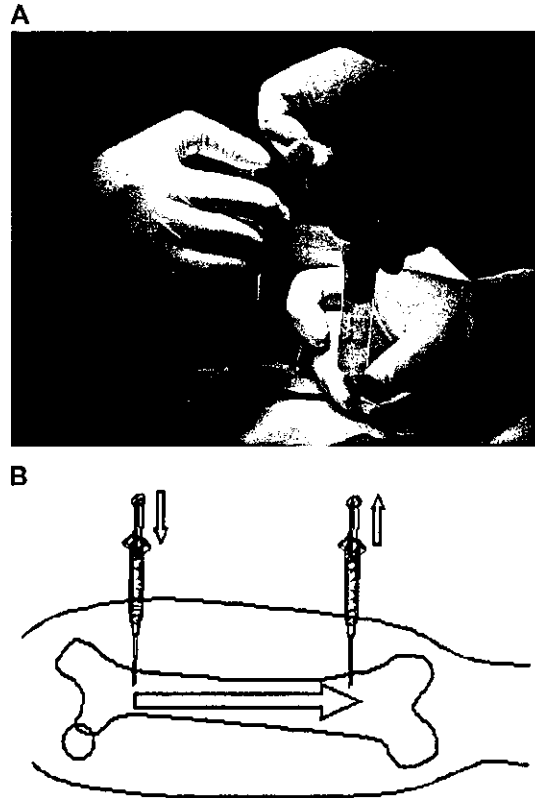

FIG. 1. The iBMT method. We inserted needles at both ends of limb bones (femurs and humeri) and irrigated the bone marrow cavity gently with saline without inflicting extra pressure (A, photo; B, schematic diagram). Gene-modified CD34^{+} cells were then injected directly into the bone marrow through the needle on one side.

After iBMT, we plated cells from the nonimplanted iliac marrow in methylcellulose medium. We examined the resulting colonies (colony-forming units, CFU) for the provirus by PCR (Fig. 2A and 2B). Two to 30% of colonies (overall 14.2% (74/522)) were positive for the

			No. of infused CD34^{+}	Fraction of provirus-positive
Animal	Target cell source	Vector	cells/kg	CFUs in infused CD34^{+} cells
		Intrabone marrow transplantation		
IB3048	Bone marrow	PLI	4.5×10^7	34/46 (73.9%)
IB3053	Peripheral blood	PLI	8.1×10^6	49/78 (62.8%)
S9042	Peripheral blood	SAG	2.6×10^7	20/35 (57.1%)
S3047	Peripheral blood	SAG	8.1×10^6	11/21 (52.4%)
D8058	Peripheral blood	SAG	7.8×10^5	11/43 (25.6%)
		PLI	5.7×10^5	9/42 (21.4%)
		Intravenous transplantation		
V0065	Peripheral blood	PLI	1.2×10^7	3/45 (6.7%)
V1007	Peripheral blood	PLI	1.5×10^6	14/41 (34.1%)

TABLE 1: *Ex vivo* transduction

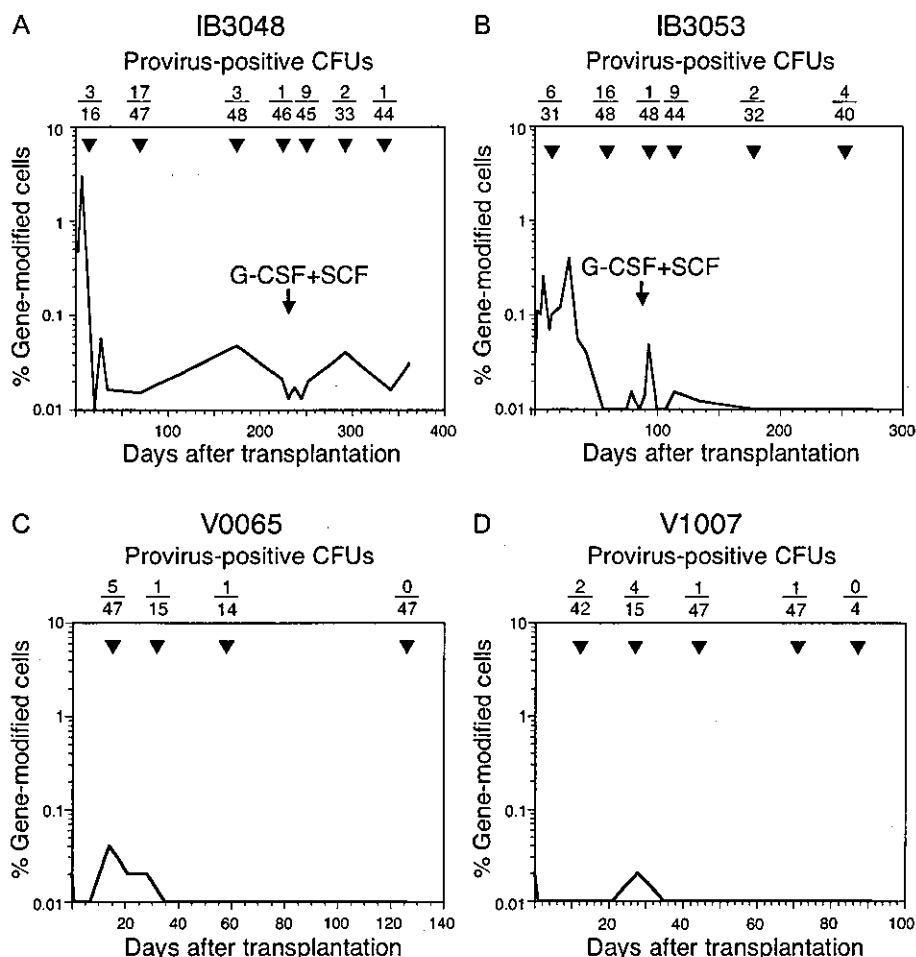PLI, nonexpression vector; SAG, selective amplifier gene vector.

470

FIG. 2. *In vivo* marking after iBMT and intravenous transplantation without marrow conditioning. CD34$^+$ cells were transduced with nonexpression retroviral vector PLI and returned by iBMT (A, IB3048, and B, IB3053) or by intravenous transplantation (C, VO065, and D, V1007) without conditioning. The upper row shows ratios of provirus-positive CFUs to β-actin-positive CFUs taken from the nonimplanted marrow at time points indicated by arrows. Overall number of provirus-positive CFUs versus overall number of β-actin-positive CFUs was 74/522 (14.2%) for iBMT (A and B) and 15/274 (5.5%) for the intravenous transplantation (C and D). The lower diagram shows percentages of gene-modified cells in the peripheral blood as assessed by quantitative PCR.

provirus and this high marking level persisted for over 1 year posttransplantation. On the other hand, after the conventional intravenous transplantation, generally fewer CFU contained the provirus (overall 5.5% (15/274)) in the bone marrow (Fig. 2C and 2D). Interestingly, the provirus in CFU from the nonimplanted marrow was detectable within 2 weeks after iBMT. Thus, transplanted cells relocated from an implanted bone to another at early time points. A similarly early translocation posttransplantation has also been reported in mouse syngeneic iBMT and human-mouse xeno-iBMT models [4,6–8]. We also examined peripheral blood cells for the provirus by quantitative PCR (Fig. 2A and 2B). The marking levels were, however, very low (<0.1%) in the peripheral blood.

Taken together, these results suggest that transplanted cells can engraft nonconditioned recipients after iBMT but their contribution to the peripheral blood is minimal compared to myeloablated recipients. The cells stay at a resting state in bone marrow without proliferation. In an attempt to proliferate and mobilize iBMT-engrafted resting progenitor cells, we administered G-

CSF and stem cell factor (SCF) for 5 consecutive days [14]; however, no obvious increase in the vector-containing cells was observed in the peripheral blood (Fig. 2A and 2B).

EPO-dependent expansion with SAG

We constructed a retroviral vector expressing an SAG that is a chimeric gene of the human EPO receptor gene (extraplus transmembrane region as a molecular switch) and the human c-Mpl gene (cytoplasmic region as a signal generator) [12]. Cells genetically engineered to express this SAG will proliferate in an EPO-dependent manner. We transduced cynomolgus CD34$^+$ cells with the SAG retroviral vector and introduced them into nonconditioned autologous recipients by iBMT (Table 1). *In vivo* results after transplantation are summarized in Table 2.

In one animal (Fig. 3A), EPO administration triggered a striking elevation in marking levels (7.4% at day 105 posttransplantation) in the peripheral blood. The level of marking in the periphery stayed high for the duration of EPO administration. After cessation of EPO, the level fell to <0.1%. Resumption of EPO administration produced a

TABLE 2: In vivo expansion with SAG after iBMT

Animal	EPO treatment Treatment course	EPO treatment Period (days posttransplant)	EPO treatment Dosage	Marked leukocytes (%)[a] Basal marking before treatment	Marked leukocytes (%)[a] Peak marking after treatment (day posttransplant)
S9042	1	1–40	200 IU/kg once daily	NA	7.36% (day 105)
		41–100	200 IU/kg twice daily	NA	7.36% (day 105)
	2	132–210	200 IU/kg twice daily	0.02%	7.72% (day 188)
	3	246–367	200 IU/kg twice daily	0.41%	8.90% (day 348)
S3047	1	75–134	200 IU/kg once daily	0.01%	0.23% (day 145)
		135–166	200 IU/kg twice daily	0.01%	0.23% (day 145)
	2	210–289	200 IU/kg twice daily	0.02%	0.00% (day 289)
D8058	1	1–86	200 IU/kg twice daily	NA	2.30% (day 14)

[a] As assessed by quantitative PCR (see Materials and Methods). NA, not applicable.

similar elevation in the marking levels. The third EPO administration again resulted in the increased marking levels to 8.9% at day 348 posttransplantation. EPO administration was associated with a mild increase in hematocrit (up to 63.5%), which was manageable by occasional phlebotomy. No other adverse effects were observed.

In another animal (Fig. 3B), the SAG-transduced cells increased following transplantation even without exogenous EPO administration. The increase may have been due to increased endogenous EPO elevation resulting from anemia present in the second animal. Overall marking fell with resolution of the anemia. Following resolution, EPO was administered, resulting in an increase in marking levels by more than 20-fold. Marking levels declined to the basal level after discontinuation of EPO. A second attempt to increase marking levels failed, with clearance of SAG-positive cells from the periphery within a month after the second administration, most likely due

to cellular immune responses to the xenogeneic SAG (see below).

Multilineage and Polyclonal Expansion

In situ PCR for the proviral sequence showed many transduced cells in the peripheral blood taken from animal S9042 receiving EPO at day 89 posttransplantation (Fig. 4A). We subjected granulocytes and T and B lymphocytes sorted from the peripheral blood of this animal at day 91 posttransplantation to semiquantitative PCR for the provirus. The provirus-containing fraction in granulocytes was 6% and that in B and T lymphocytes was 2% (Fig. 4B), thus indicating that multilineage expansion had occurred. The persistence of marked, short-lived granulocytes for the long term is also another evidence of the successful engraftment of gene-modified HSCs after iBMT. The integration site analysis using the linear amplification-mediated (LAM) PCR method [15]
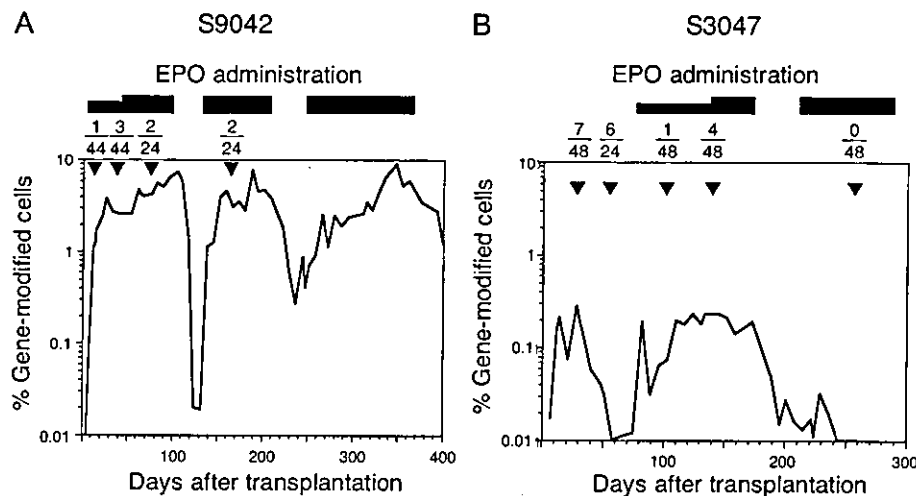

FIG. 3. Expansion of SAG-transduced cells by treatment with EPO after iBMT. CD34+ cells transduced with SAG were returned to each animal by iBMT without conditioning. The animals (A) S9042 and (B) S3047 received EPO at 200 IU/kg once or twice daily (indicated by closed bars). The upper row shows ratios of provirus-positive CFUs to β-actin-positive CFUs taken from the nonimplanted marrow at time points indicated by arrows. The lower diagram shows percentages of gene-modified cells in the peripheral blood as assessed by quantitative PCR.

472